This is to certify that the

thesis entitled

A Comparative Study in
Automotive Active Suspension Systems

presented by

Yung-Chi Lin

has been accepted towards fulfillment
of the requirements for

Master's degree in Electrical Engineering

Hassan Khalil
Major professor

Date April 10, 1992

A COMPARATIVE STUDY

IN

AUTOMOTIVE ACTIVE SUSPENSION SYSTEMS

By

Yung-Chi LIN

A THESIS

Submitted to
Michigan State University
in partial fulfillment of the requirements
for the degree of

MASTER OF SCIENCE

Department of Electrical Engineering

1992

ABSTRACT

A COMPARATIVE STUDY IN AUTOMOTIVE ACTIVE SUSPENSION SYSTEMS

By

Yung-Chi LIN

The vehicle active suspension problem is investigated using a quarter car model which consists of one fourth of the body mass, suspension components and one wheel. A State space approach is used and three control methodologies including LQG/LTR, constant gain output feedback and singular perturbation are applied. The performance criteria of suspension systems are formulated into minimizing sprung mass acceleration, suspension deflection, and tire deflection for the concerns of ***ride comfort***, ***working space constraint***, and ***road holding ability***, respectively. Various measurement schemes which contain position, velocity and acceleration are investigated. It is shown that sprung mass acceleration gain can be attenuated significantly over a wider frequency band, reaching into the wheel resonance via using acceleration feedback, then characterizing the dynamics into slow and fast models and designing compensators individually to meet desired specifications for low and high frequency ranges. Nonideal integration, controller bandwidth, force level requirement and robustness are also studied. All designs demonstrate comparable robustness properties when system parameters are perturbed.

To my Parents

For their affection and devotion

ACKNOWLEDGMENTS

I am grateful to my advisor, Dr. Hassan K. Khalil, for inspiring and instructing me all the way through this research. His patience and provocative insights have been major motivations for this thesis. With his help through the many stages where I got stuck with my progress, I came to realizing my potential in doing research.

I want to thank Dr. G. L. Park and Dr. R. L. Tummala for their time and energy to be the members of my thesis committee.

My deepest respect and gratitude go to my wife, Tsailing Liang, for her constant love, encouragement, and sacrifice. She has tried every means possible to help me concentrate on doing my research, even in her poor health after our first baby, Alexander, was born on Oct 1st, 1991.

I really owe thousands of thanks to many people in the world – mentioned or not mentioned in this acknowledgement.

Contents

List of Tables

List of Figures

Chapter 1

Active Suspension

The automotive industry is always pursuing more comfortable and safer cars. Improvement in suspension systems plays an important role in achieving these goals. Naturally, the suspension system is then expected to have more intelligence to accommodate itself in various road conditions. The increasing capability and decreasing cost of electronic components motivate people's strong interest in this topic.

1.1 What Is Active Suspension?

An active suspension system is considered as one with the following two features [1].

1. Energy is constantly supplied to the suspension system and the force generated by that energy is constantly controlled.

2. The suspension system incorporates various types of sensors and a unit for processing signals; it generates forces which are functions of the output signals.

One possible structure of active suspension systems is depicted in Fig.1. The system employs sensors to measure signals, a compensator to process signal and an electro-hydraulic actuator to generate force. Shown in this figure is the so-called quarter car model consisting of one fourth of the body mass, suspension components and one wheel. The model describes the $y - axis$ motion under road disturbances when the vehicle moves in the $x - axis$ direction. It does not describe other motions of the body like roll or pitch.

1.2 Classification of Suspension Systems

The design of traditional suspension systems requires a careful choice of spring and damper which are assumed to behave linearly. This system is referred to as *passive suspension system* (PSS) since no external energy is added to generate any control force. An *active suspension system* (ASS) usually employs an electrohydraulic system to achieve its performance criteria, requiring extra power supply and a signal processing unit. Another kind of suspension system between the previous two systems is called *semi-active suspension system* (SAS). Based on different control laws, the damper of the SAS can be switched on/off or adjusted continuously to meet various road conditions. It does not require power supply as large as the ASS. This will introduce nonlinear characteristics into the system. Some research [3, 4, 5, 6] has been dedicated to the study of SAS.

1.3 Mathematical Model

The quarter car model used in this thesis is shown in Fig.1. The state variables are chosen as follows [12],

$$x = \begin{bmatrix} z_s - z_u \\ \dot{z}_s \\ z_u - z_r \\ \dot{z}_u \end{bmatrix} \tag{1.1}$$

where $z_s - z_u$, $\dot{z}_s$, $z_u - z_r$ and $\dot{z}_u$ are, respectively, called *suspension deflection, sprung mass velocity, tire deflection* and *tire velocity.* The state space equation is then given by

$$\dot{x} = Ax + Bu + E\dot{z}_r \tag{1.2}$$

where

$$A = \begin{bmatrix} 0 & 1 & 0 & -1 \\ -k_s/m_s & -b_s/m_s & 0 & b_s/m_s \\ 0 & 0 & 0 & 1 \\ k_s/m_u & b_s/m_u & -k_t/m_u & -b_s/m_u \end{bmatrix}, B = \begin{bmatrix} 0 \\ 1/m_s \\ 0 \\ -1/m_u \end{bmatrix}, E = \begin{bmatrix} 0 \\ 0 \\ -1 \\ 0 \end{bmatrix} \tag{1.3}$$

The above vehicle parameters are defined in Fig.1. In our study, a typical set of vehicle parameters shown in Table 1.1 is taken from [2].

$m_s = 504.5kg$
$m_u = 62kg$
$b_s = 1328N.s/m$
$k_s = 13100N/m$
$k_t = 252000N/m$

Table 1.1: Vehicle Parameters

When active control is used, the damping constant, b_s, is replaced by $400 N.s/m$. The damper is not completely removed due to a practical safety concern in case of the failure of the control system. The observed outputs of interest are *position* (suspension deflection, $z_s - z_u$), *velocity* (sprung mass velocity, $\dot{z}_s$) and *acceleration* (sprung mass acceleration, $\ddot{z}_s$). The suspension deflection can be measured by acoustic or radar transmitter & receiver; while the velocity $\dot{z}_s$ is typically obtained by integrating the acceleration $\ddot{z}_s$ which is measured using accelerometer [16].

1.4 Performance Measure

Traditionally, a good suspension system is supposed to be able to provide passengers with ride comfort, while maintaining necessary road holding ability to satisfy maneuvering safety concerns, subject to the design constraint of limited suspension working space. Ride comfort is related to vehicle body motion sensed by passengers and, generally, measured by vehicle body acceleration (sprung mass acceleration for the quarter car model). Road holding ability is affected by wheel load dynamic variations, i.e., fluctuation of the contact force between the tire and the road surface. Clearly, this fluctuation is directly related to tire deflection. When road disturbances come into the suspension system, the relative displacement between the body and wheel keeps varying in such a way that the disturbance transmission is kept as small as possible, to provide best comfort. However, the allowable relative displacement is limited by the usable working space. Thus, the previous discussions lead us to formulate the performance criteria into minimizing sprung mass acceleration, suspension deflection, and tire deflection for *ride comfort, working space constraint*, and *road holding ability* [9, 10, 11, 12, 13, 14], respectively. It is well known that there is always a trade-off in minimizing these performance criteria [9, 10, 11, 12, 13, 14]. In this research, control effort, force actuator bandwidth, robustness and nonideal signal processing in using *velocity* feedback are also considered. Hrovat [7] has identified the advantages of taking jerk (derivative of acceleration) into consideration for ride comfort, but his idea has not yet received much support.

1.5 Organization of Thesis

This thesis is organized into six chapters. The first chapter is an introduction to the active suspension system, including the mathematical model description, and the performance measure of suspension systems. Chapter 2 reviews some control methodologies of LQR, LQG, and constant gain output feedback. The simulation results with the applications of the above methodologies are also presented under velocity and position feedback. The value of acceleration feedback is first explored with LQG method in chapter 3. Chapter 4 introduces the singularly perturbed systems and the sequential design procedure. Two sequential design examples are presented in this chapter. A comprehensive study of the above schemes is performed in chapter 5. The issues discussed in this chapter include nonideal integration, performance evaluation, controller bandwidth, force level, and robustness. The robustness is investigated via evaluating both the singular values of the complementary sensitivity functions and the performance under system parameter perturbations. Chapter 6 presents conclusions. For the purpose of comparison, some performance results reported in other literature are also mentioned briefly.

Chapter 2

Review of Some Control Strategies

In this chapter, the theory of LQR, LQG [8] and constant gain output feedback are briefly described. The performance of ASS by the application of LQR is evaluated as a reference performance. After that, with the observed outputs of position and velocity, LQG designs and output feedback are done. In doing LQG designs, the concept of LQG/LTR (Loop Transfer Recovery) is introduced to achieve the desired frequency loop shaping. The work of LQG is similar to the work of [12]; the work of constant output feedback is similar to [2].

2.1 Linear Quadratic Regulator (LQR)

Consider the system

$$\dot{x} = Ax + Bu \tag{2.1}$$

Assuming measurements of all states available, the LQR problem can be formulated into seeking a linear control law

$$u = -Gx \tag{2.2}$$

where G is a suitable stabilizing gain matrix, to minimize the performance index

$$PI = \int_0^\infty (x'Qx + u'Ru)\, d\tau \tag{2.3}$$

R is a positive definite symmetric matrix and Q is a positive semidefinite symmetric matrix. It is well known that the optimal gain, G, is given by

$$G = R^{-1}B'M \tag{2.4}$$

where M satisfies the *algebraic Riccatic equation* (ARE)

$$0 = MA + A'M - MBR^{-1}B'M + Q \tag{2.5}$$

When (A, B) is controllable and $(A, \sqrt{Q})$ is observable, the Riccatic equation (2.5) has a unique solution $M = M' > 0$ such that $(A - BR^{-1}B'M)$ is Hurwitz.

2.2 Linear Quadratic Gaussian (LQG)

Consider the state equation

$$\dot{x} = Ax + Bu + Ev \tag{2.6}$$

and the observed output equation

$$y = Cx + w \tag{2.7}$$

where v and w are Gaussian *white* noise processes with

$$E\left[v(t)v(t+\tau)\right] = \delta(\tau), E\left[w(t)w(t+\tau)\right] = \mu\delta(\tau) \tag{2.8}$$

The LQG problem seeks an optimal control u that minimizes the performance index

$$PI = \lim_{T\to\infty} \frac{1}{T} E\{\int_0^T (x'Qx + u'Ru)\, d\tau\} \tag{2.9}$$

The optimal solution of the LQG problem is given by

$$u = -G\hat{x} \tag{2.10}$$

where G is the same optimal control gain defined by Equation (2.4), and $\hat{x}$ is the optimal state estimate, defined by the optimal observer or Kalman filter

$$\dot{\hat{x}} = A\hat{x} + Bu + K(y - C\hat{x}) \tag{2.11}$$

The observer gain K is given by

$$K = \frac{1}{\mu} P C' \tag{2.12}$$

where P satisfies the ARE

$$0 = AP + PA' - \frac{1}{\mu} P C' C P + E E' \tag{2.13}$$

Although μ indicates the value of the sensor noise, it is often treated as a design parameter to reflect the bandwidth of the observer. By increasing the bandwidth of the observer, i.e. $\mu \rightarrow 0$, the feedback loop transfer function of an LQR system can be recovered by an LQG system. This is the so-called LQG/LTR (Loop Transfer Recovery) methodology [23, 26].

2.3 LQG Applied to ASS

Looking at the system dynamic equation (1.2), there are two inputs coming into the picture. The design task is to select a control u to reject the effect of the road disturbance $\dot{z}_r$ on the sprung mass acceleration $\ddot{z}_s$.

Fig.2 shows the frequency response of the original passive system. It is easily noticed that the suspension system dynamics contain two distinct oscillatory modes: one mode corresponds to body resonance ($\approx$ 1 Hz); the other corresponds to wheel resonance ($\approx$ 10 Hz). The damping constant of the passive system is $1328 N.s/m$ which will be replaced by a smaller value of $400 N.s/m$ when control is applied. As stated previously, the reference performance is designed by an LQR procedure [8].

The following Q and R

$$Q = diag[\ 0 \quad 1225 \quad 0 \quad 156\ ] \tag{2.14}$$

$$R = [0.000056] \tag{2.15}$$

yield the state feedback gain G, given by

$$G = [\ 0 \quad 4374 \quad -14448 \quad -1274\ ] \tag{2.16}$$

which will be used in cascade with observer. In particular, both the states $z_u - z_r$ and $\dot{z_u}$ are not easily measured. The LQG design is used, assuming only position $(z_s - z_u)$ or velocity $(\dot{z_s})$ are available. The observer equation is then given by

$$\dot{\hat{x}} = A\hat{x} + Bu + K(y - C\hat{x}) \tag{2.17}$$

with the measured output being

$$y_{position} = C_p x + w = [\ 1 \quad 0 \quad 0 \quad 0\ ]x + w \tag{2.18}$$

or

$$y_{velocity} = C_v x + w = [\ 0 \quad 1 \quad 0 \quad 0\ ]x + w \tag{2.19}$$

In order to apply LQG, the road velocity $\dot{z_r}$ and sensor noise w are modelled as *white* noise processes, i.e.,

$$E\left[\dot{z_r}(t)\dot{z_r}(t+\tau)\right] = \delta(\tau), E\left[w(t)w(t+\tau)\right] = \mu\delta(\tau) \tag{2.20}$$

As stated in Sec.2.2, μ is used as a design parameter to determine the bandwidth of the observer. In Fig.3 and Fig.4 the LTR results are seen. The dotted lines indicate the performance of LQR designs. Table 2.1 shows the values of μ used in these Figures.

$\mu(Pos.)$	10^{-3}	10^{-4}	5×10^{-5}	10^{-6}
$\mu(Vel.)$	10^{-3}	10^{-4}	5×10^{-5}	10^{-6}

Table 2.1: LTR μ of LQG-P and LQG-V

The arrows in these plots indicate the corresponding directions of change. It is easily noticed that larger suspension deflection $z_s - z_u$ and high frequency tire deflection $z_u - z_r$ come along with the improvement of sprung mass acceleration $\ddot{z}_s$ and low frequency tire deflection. Based on the principle of "equal working space [1]", the design parameters are picked up as in Table 2.2. Once the design parameter μ is picked up, the observer is determined. The frequency response of the LQG-P and LQG-V designs are shown in Fig.6. Note that the suspension deflections $z_s - z_u$ are very close to each other.

2.4 Constant Gain Output Feedback (CGOF)

CGOF has been applied in [2] by the centralized/local optimization procedures to solve a full car ASS problem. Motivated by this idea, CGOF is used to investigate various measurements. The control is obtained by multiplying measured signals with a constant gain, denoted by K_c. In single-input–single-output systems, K_c is scalar.

[1]This principle is discussed in [11]. It is primarily to express a common usable space constraint which exists in designing vehicle suspension systems. Even when active control are applied, it is still considered as a fair comparison baseline for various designs.

$\mu(Position)$	0.0001
$\mu(Velocity)$	0.000075

Table 2.2: Designed μ of LQG-P and LQG-V

This fact simplifies our analysis.

Consider a system

$$\dot{x} = Ax + Bu \tag{2.21}$$

$$y = Cx + Du \tag{2.22}$$

where u and y are scalar variables. Suppose the control u is obtained by

$$u = -K_c y = -K_c(Cx + Du) = -K_c Cx - K_c Du \tag{2.23}$$

if $I + K_c D$ is nonsingular, then

$$u = -(I + K_c D)^{-1} K_c C x \tag{2.24}$$

The closed loop system is represented by

$$\dot{x} = (A - B(I + K_c D)^{-1} K_c C)x \tag{2.25}$$

Since K_c is scalar, the stabilizing range of K_c can be determined by looking at the root locus of the closed loop system. Therefore, we study all possible values of K_c to pinpoint a satisfactory K_c for each of the different measurement schemes. The root locus analysis of CGOF for various measurements shows that only velocity feedback can provide with enough damping force. Thus, only the results of velocity feedback will be discussed.

Fig.8 shows the performance of several CGOF designs. Table 2.3 summarizes the values of K_c used in this Figure. Likewise, the arrows in this Figure indicate the corresponding directions of change. Both of the open loop performance and LQR are also shown for comparison. For convenience, the root locus of position,velocity and acceleration feedback schemes are reported in Fig.9. Note that, for the case of velocity feedback, the two fast poles are insensitive to K_c range of interested, as shown in Table 2.3. In other words, when K_c is tuned not greater than 20000, their motions toward imaginary axis are negligible. This characterizes the CGOF loop shaping primarily in low frequency range. Note that the performance changes only in

K_c	1000	5000	10000	20000

Table 2.3: Designing K_c of CGOF systems

the low-frequency range when K_c varies, i.e., the high frequency shape of open loop system is still kept in feedback system. This scheme increases damping force around body resonance to eliminate the two body resonance peaks of acceleration and tire deflection. Compared to the LQR performance, the price paid in larger suspension deflection and high frequency tire deflection is also observed.

Chapter 3

Acceleration Feedback

The output feedback controllers designed in the previous chapter use measurements of suspension deflection $z_s - z_u$ (LQG-P) or the sprung mass velocity $\dot{z}_s$ (LQG-V & CGOF). The suspension deflection can be measured by acoustic or radar transmitter & receiver; while the velocity $\dot{z}_s$ is typically obtained by integrating the acceleration $\ddot{z}_s$ which is measured using accelerometer [16]. This integration scheme shows that the actual observed output is acceleration, and requires an integrator part in cascade with the compensator designed using velocity feedback. The nonideal effects of such integration have been discussed in [17]. The restriction of the controller to have an integral component might be limiting the performance which can be achieved with a more general use of acceleration feedback. Hence, the design of LQG controller using acceleration feedback is explored in this chapter.

3.1 LQG with Acceleration Feedback (LQG-A)

In order to use sprung mass acceleration $\ddot{z}_s$ which is given by

$$\ddot{z}_s = [\ -k_s/m_s \quad -b_s/m_s \quad 0 \quad b_s/m_s\ ]x + [1/m_s]u \tag{3.1}$$

Equations (2.7) and (2.11) are modified as follows.

$$y = Cx + Du + w \tag{3.2}$$

$$\dot{\hat{x}} = A\hat{x} + Bu + K(y - \hat{y}) \tag{3.3}$$

where

$$\hat{y} = C\hat{x} + Du \tag{3.4}$$

3.2 Performance of LQG-A

The LQG/LTR design performance for the acceleration feedback are shown in Fig.7 with the design parameters μ shown in Table 3.1, where $\mu = 1.0$ is picked up for LQG-A design.

$\mu(Acc.)$	10.0	2.0	1.0	0.1

Table 3.1: LTR μ of LQG-A

The observer gain K and design parameter μ of the three LQG designs are summarized in Table 3.2. Looking at Fig.6 and Fig.7, the LQG-A design used in this work does not provide with remarkable advantages over the LQG-P and LQG-V designs. The reasons will be discussed in chapter 5. Compared to the performance of LQG-V & LQG-P, the LQG-A design has a smaller suspension deflection $z_s - z_u$ along with

type	K'				μ
LQG-P	[103.80	-82.3	-4.20	-5474.40]	0.0001
LQG-V	[-123.70	127.1	9.20	6262.10]	0.00075
LQG-A	[-0.72	0.0	-0.27	53.58]	1.0

Table 3.2: Observer Gain K for Various Schemes

a sacrifice in sprung mass acceleration and tire deflection.

Chapter 4

Singular Perturbation Approach

In vehicle suspension systems, the presence of body (slow) and wheel (fast) resonance shows the existence of a two-time-scale structure [21]. This can be utilized by the application of singular perturbation methodology. In this chapter, a brief description of singularly perturbed systems and the sequential design procedure of [18] is first presented. The suspension system is then cast into a singularly perturbed form which is composed of two submodels called *slow* and *fast* models. The value of using acceleration feedback is easily seen at this point because the transfer function from the control input to the acceleration output has nontrivial slow and fast components. The corresponding transfer functions for position and velocity outputs have zero fast models. This chapter concludes with two design examples where the sequential design procedure is employed to design the acceleration feedback controllers.

4.1 Singularly Perturbed Systems

A linear time-invariant singularly perturbed system is represented by

$$\dot{x} = A_{11}x + A_{12}z + B_1u \tag{4.1}$$

$$\epsilon\dot{z} = A_{21}x + A_{22}z + B_2u, det\,[A_{22}(0)] \neq 0 \tag{4.2}$$

$$y = C_1x + C_2z + Du \tag{4.3}$$

where $x \in R^n$ denotes the *slow* state vector; $z \in R^m$ denotes the *fast* state vector; $u \in R^p$ is the control input and $y \in R^q$ is the output. The separation between the slow and fast dynamics can be represented by the small positive constant ϵ in the sense that $\dot{x}$ is $O(1)$, whereas $\dot{z}$ is $O(\frac{1}{\epsilon})$. In other words, as $\epsilon \rightarrow 0$, the singularly perturbed system of (4.1)–(4.3) has a two-time-scale structure and the eigenvalues cluster into a group of slow $O(1)$ eigenvalues and a group of fast $O(\frac{1}{\epsilon})$ eigenvalues. The *full* system can be approximated by the slow and fast models.

The slow model is given by

$$\dot{x}_s = A_0x_s + B_0u \tag{4.4}$$

$$y_s = C_0x_s + D_0u \tag{4.5}$$

where $A_0 = A_{11} - A_{12}A_{22}^{-1}A_{21}, B_0 = B_1 - A_{12}A_{22}^{-1}B_2, C_0 = C_1 - C_2A_{22}^{-1}A_{21}$ and $D_0 = D - C_2A_{22}^{-1}B_2$. The fast model is given by

$$\dot{z}_f = A_fz_f + B_fu \tag{4.6}$$

$$y_f = C_fz_f + D_fu \tag{4.7}$$

where $A_f = A_{22}/\epsilon, B_f = B_2/\epsilon, C_f = C_2$, and $D_f = D$. Various properties of the singularly perturbed system (4.1)–(4.3) can be approximated by the slow and fast models (4.4)–(4.7). Two approximations that are used in this paper are the eigenvalue and transfer function approximations.

Eigenvalue Approximation [20]

As $\epsilon \to 0$ the slow eigenvalues of the full singularly perturbed system (4.1)–(4.3) approach the eigenvalues of the slow model of (4.4)–(4.5); the fast eigenvalues of (4.1)–(4.3) approach the eigenvalues of the fast model of (4.6)–(4.7).

Transfer Function Approximation [19]

The transfer function, denoted by $G(s,\epsilon)$, of the full singularly perturbed system (4.1)–(4.3) can be approximated by

$$G(s,\epsilon) = G_s(s) + G_f(\epsilon s) - G_s(\infty) + O(\epsilon) \tag{4.8}$$

on the imaginary axis $s = jw$, where $G_s(s)$ and $G_f(\epsilon s)$ denote the transfer functions of the slow and fast models, respectively, i.e.,

$$G_s(s) = C_0(sI - A_0)^{-1}B_0 + D_0$$

$$G_f(\epsilon s) = C_f(sI - A_f)^{-1}B_f + D_f = C_2(\epsilon sI - A_{22})^{-1}B_2 + D$$

Equation (4.8) is valid when $G_s(s)$ and $G_f(\epsilon s)$ have no poles on the imaginary axis, which is the case when they are stable.

4.2 Sequential Design Procedure

A stabilizing output feedback compensator, with two-time-scale structure, can be obtained by the following sequential design procedure [18].

1. Design a fast compensator $C_f(\epsilon s)$ to stabilize the high frequency feedback loop $[C_f(\epsilon s), G_f(\epsilon s)]$ and to meet high-frequency design specifications.

2. Design a slow compensator $C_s(s)$ to stabilize the low-frequency feedback loop $[C_s(s), G_s(s)]$ and to meet low-frequency design specifications, subject to the constraint

$$C_s(\infty) = C_f(0) \tag{4.9}$$

3. A composite compensator $C(s,\epsilon)$, taken as the parallel connection of $C_f(\epsilon s)$ and the strictly proper part of $C_s(s)$, will stabilize the closed-loop system $[C(s,\epsilon), G(s,\epsilon)]$ for sufficiently small ϵ. Moreover, any point to point the transfer function of the closed loop system $[C(s,\epsilon), G(s,\epsilon)]$ is $O(\epsilon)$ close to the one approximated by the corresponding slow and fast models, as stated in (4.8).

4.3 Modeling in Singular Perturbation (SPT)

In vehicle suspension systems, the time scale characteristics are composed of two resonance modes: body resonance and wheel resonance [21]. To apply singular perturbation theory, a singularly perturbed model of suspension systems is needed. First, the small positive constant, ϵ, which represents the separation of the slow and fast dynamics can be chosen as the ratio between sprung mass resonance and unsprung mass resonance, i.e.,

$$\epsilon = \frac{\sqrt{k_s/m_s}}{\sqrt{k_t/m_u}} \tag{4.10}$$

For the typical data of Table 1.1, $\epsilon \approx 0.1$. It is shown in the Appendix that the suspension system is a singularly perturbed system with the first two state variables, $z_s - z_u$ and $\dot{z}_s$ as *slow* variables and the other two state variables, $z_u - z_r$ and $\dot{z}_u$ as *fast* variables. Hence, assuming acceleration measurement

$$\ddot{z}_s = \begin{bmatrix} -k_s/m_s & -b_s/m_s & 0 & b_s/m_s \end{bmatrix} x + [1/m_s]\, u = Cx + Du \tag{4.11}$$

and using the vehicle parameters given in Table 1.1, the *full* system can be approximated by the slow and fast models given below.

Slow model

$$A_0 = A_{11} - A_{12}A_{22}^{-1}A_{21} = \begin{bmatrix} 0 & 1 \\ -25.97 & -0.79 \end{bmatrix}, B_0 = B_1 - A_{12}A_{22}^{-1}B_2 = \begin{bmatrix} 0 \\ 0.002 \end{bmatrix}$$

$$C_0 = C_1 - C_2A_{22}^{-1}A_{21} = \begin{bmatrix} -25.97 & -0.79 \end{bmatrix}, D_0 = D - C_2A_{22}^{-1}B_2 = [0.002] \tag{4.12}$$

Fast model

$$\begin{gathered} A_f = \begin{bmatrix} 0 & 1 \\ -4064.5 & -6.5 \end{bmatrix}, \quad B_f = \begin{bmatrix} 0 \\ -0.016 \end{bmatrix}, \\ C_f = \begin{bmatrix} 0 & -0.793 \end{bmatrix}, \qquad D_f = [0.002] \end{gathered} \tag{4.13}$$

The value of using acceleration feedback is seen from the fact that the measurement matrices C_f & D_f in the fast model are nonzero. Consequently, the fast model $G_f(\epsilon s)$ is not trivial. If position or velocity feedback is used, i.e.,

$$y_{position} = \begin{bmatrix} 1 & 0 & 0 & 0 \end{bmatrix} x, \quad y_{velocity} = \begin{bmatrix} 0 & 1 & 0 & 0 \end{bmatrix} x$$

we have

$$C_{f,velocity} = C_{f,position} = 0, \quad D_{f,velocity} = D_{f,position} = 0$$

Hence, the fast model $G_f(\epsilon s)$ will be identically zero, and feedback will have a little effect on the performance of the system in the high-frequency range. More precisely, the effect of feedback on the closed-loop transfer function in the high-frequency range will be $O(\epsilon)$. In the case of acceleration feedback, the fast model in not trivial and feedback could have a significant effect in the high-frequency range.

Eigenvalue Approximation

The eigenvalue approximation for the open loop system is demonstrated in Table 4.1.

Eigenvalues	*fast*	*slow*
Approximate	$-3.23 \pm 63.67j$	$-0.40 \pm 5.08j$
Exact	$-3.26 \pm 65.28j$	$-0.36 \pm 4.86j$

Table 4.1: Eigenvalue Approximation for the Open Loop System

Transfer Functions Approximation

Fig.10–Fig.15 show the frequency response of the transfer functions of the system from control force, u, and road velocity, $\dot{z}_r$, to the three controlled outputs. They are shown in the order of (1) slow, (2) fast, (3) composite and (4) full. In the case of Fig.11 & Fig.14, **the fast transfer function is identically zero**. The composite transfer function is $O(\epsilon)$ close to the full transfer function. It is easily noticed that there is a "sharp dip" at the point of wheel resonance in the transfer function of u to $\ddot{z}_s$. This implies that the control u has no (or *very little*) influence on the ride comfort at that frequency point. That point is referred to as the *Invariant Point*, and the fact that it cannot be changed by feedback is proved in [12].

4.4 Sequential Design Example I (SPT-2)

4.4.1 Fast Design

Under sprung mass acceleration feedback, with a lighter damper, $b_s = 400 N.s/m$, the fast subsystem is not a strictly proper plant as given below:

$$G_{fast}(s) = \frac{0.002s^2 + 8.0565}{s^2 + 6.5s + 4064.5} \tag{4.14}$$

The fast transfer function is written in terms of s rather than ϵs since the parameter ϵ is substituted in the fast model by its numerical value. Under the consideration of controller order not exceeding plant order, a constant gain controller is first tried and causes instability. Therefore, in order to improve stability and satisfy the well-posedness requirement [22], a controller with one zero and two poles is proposed for the fast subsystem. The transfer function of this controller is in the form

$$C_{fast}(s) = K\frac{s + z}{s^2 + 2\zeta w_n s + w_n^2} \tag{4.15}$$

Using root-locus (Fig.16) and Bode plot techniques, the following compensator parameters are chosen, with emphasis on ride comfort improvement:

$$K = 180000, z = 36, \zeta = 0.5, w_n = 100 \tag{4.16}$$

4.4.2 Slow Design

The transfer function of the slow subsystem is

$$G_{slow}(s) = \frac{0.002s^2}{s^2 + 0.7929s + 25.9663} \tag{4.17}$$

In the low frequency range, the design task is to choose a slow controller to meet the slow design damping force requirements and eliminate the resonance peak, subject to the following constraint:

$$C_{slow}(\infty) = C_{fast}(0) = 648 \tag{4.18}$$

In order to satisfy the above constraint, the proposed controller is taken in the form

$$C_{slow}(s) = 648\left(\frac{z}{s+p} + 1\right) \tag{4.19}$$

For the concern of the separation of the slow and fast dynamics, the choice of the zero and the pole should not exceed the mid-point between the sprung and unsprung mass resonance frequencies, which is about 5 Hz. Using root locus (Fig.16) and Bode plot, the slow compensator is taken as

$$C_{slow}(s) = 648\left(\frac{12}{s+0.8} + 1\right) \tag{4.20}$$

4.4.3 Full Design

The two-time-scale stabilizing controller is taken as the parallel connection of $C_{fast}(s)$ and the strictly proper part of $C_{slow}(s)$, i.e.

$$\begin{aligned} C(s) &= C_{slow}(s) + C_{fast}(s) - C_{slow}(\infty) \\ &= 648 \times \frac{12}{s+0.8} + 180000 \times \frac{s+36}{s^2+100s+100^2} \end{aligned} \tag{4.21}$$

The full design is applied to the system. The closed-loop performance of the full system (under the composite compensator (4.21)) is shown in Fig.17. The closed-loop eigenvalues are summarized in Table 4.2.

It is noticed that a very wide band reduction and a very sharp wheel resonance

fast	-426.16	-46.85	$-0.77 \pm 64.24i$
slow	-10.55	$-0.57 \pm 0.8i$	

Table 4.2: Closed Loop Eigenvalues of SPT-2

reshaping in sprung mass acceleration have been achieved. This significant improvement, however, introduces other lightly damped peaks in suspension and tire defection, which implies larger working space and worse road holding ability. Actually, the necessity of high peak force level at wheel resonance is also noticed, which will be mentioned later. Due to the concern of actuator saturation, a force roll-off might be preferred in high frequency range. Thus, the performance of SPT-2 might not be satisfactory enough.

4.5 Sequential Design Example II (SPT)

In the previous section, the restriction of controller order not exceeding plant is imposed on the fast design, and results in a pair of lightly damped poles which are responsible for several undesirable peaks. This restriction will be relaxed a little bit but still imposed on the full system in this section, i.e., a 3^{rd} order fast controller and a 1^{st} order slow controller will be considered.

4.5.1 Fast Design

Under sprung mass acceleration feedback, with a lighter damper, $b_s = 400N.s/m$, the fast subsystem is repeated below:

$$G_{fast}(s) = \frac{0.002s^2 + 8.0565}{s^2 + 6.5s + 4064.5} \tag{4.22}$$

which has two zeros at $\pm 63.46j$ and two poles at $-3.23 \pm 63.67j$. A 3^{rd} controller with two zero and three poles is considered for the fast subsystem. The transfer function of this controller is in the form of

$$C_{fast}(s) = K\frac{s^2 + 2\zeta_z w_{nz} s + w_{nz}^2}{(s^2 + 2\zeta_p w_{np} s + w_{np}^2)(s + p)} \tag{4.23}$$

Under stability and well-posedness concerns as stated previously, the design idea is to choose a pair of complex zeros around the neighborhood of the fast poles to keep the open loop high frequency damping characteristics; while the choice of the poles is done without causing another significant resonance. Moreover, due to the actuator behaviors, the high frequency ride comfort improvement is also desired while not increasing force level in that range. As shown in the lower half of Fig.18, the open loop fast poles move slightly left before meeting with the controller poles. If the controller gain is appropriately chosen, the open loop high frequency damping is then expected to be preserved. This leads us to choose the following compensator:

$$C_{fast}(s) = 54000\frac{s^2 + 7.5s + (65.8)^2}{(s^2 + 60.5s + (72.0)^2)(s + 30)} \tag{4.24}$$

4.5.2 Slow Design

The transfer function of the slow subsystem is repeated again

$$G_{slow}(s) = \frac{0.002s^2}{s^2 + 0.7929s + 25.9663} \tag{4.25}$$

In the low frequency range, the design task is to choose a slow controller to meet the slow design damping force requirement and eliminate the resonance peak, subject to the following constraint:

$$C_{slow}(\infty) = C_{fast}(0) = 1504 \tag{4.26}$$

In order to satisfy the above constraint, the proposed controller is taken in the form of

$$C_{slow}(s) = 1504(\frac{z}{s+p} + 1) \tag{4.27}$$

Likewise, for the separation concern of the slow and fast dynamics, the choice of the zeros and the pole should not exceed the mid-point between the sprung and unsprung mass resonance frequencies which is about 5 Hz. The slow compensator is taken as

$$C_{slow}(s) = 1504(\frac{7}{s+0.8} + 1) \tag{4.28}$$

4.5.3 Full Design

The two-time-scale stabilizing controller can be taken as the parallel connection of $C_{fast}(s)$ and the strictly proper part of $C_{slow}(s)$, i.e.

$$\begin{aligned} C(s) &= C_{slow}(s) + C_{fast}(s) - C_{slow}(\infty) \\ &= 1504\frac{7}{s+0.8} + 54000\frac{s^2 + 7.5s + (65.8)^2}{(s^2 + 60.5s + (72.0)^2)(s+30)} \end{aligned} \tag{4.29}$$

The full design is applied to the system. The closed-loop eigenvalues are summarized in Table 4.3. Note that the open loop fast poles, $-3.26 \pm 65.28j$ (shown in Table 4.1), have been moved to $-3.59 \pm 65.87j$. Thus, the fast open loop damping is preserved in this design. The closed-loop performance of the slow, fast, and full systems (under the composite compensator (4.29)) is shown in Fig.19. For the purpose of comparison, the same transfer functions are shown under the passive system. The performance of SPT

fast	-192.18	$-3.59 \pm 65.87j$	$-10.84 \pm 60.68j$
slow	-4.35	$-0.55 \pm 0.84j$	

Table 4.3: Closed Loop Eigenvalues of SPT

and SPT-2 are shown in Fig.20 & Fig.21 again. Compared to SPT-2, the undesirable peaks including high frequency tire deflection, suspension deflection, and force level are reduced. Although a sharp reduction in high frequency sprung mass acceleration is lost, we still have some more ride comfort and road holding improvement at the low frequency range (below 5 Hz). Generally speaking, SPT performs more satisfactorily than SPT-2.

Chapter 5

Comparative Study

Five controllers have been designed. They are LQG-P, LQG-V, LQG-A, CGOF and SPT. A comparative study in those various control schemes will be done in this chapter based on the perspectives of nonideal integration, controller bandwidth, actuator force level requirement and system robustness.

5.1 Nonideal Acceleration Integration

Velocity signal is typically obtained by integrating acceleration. The practical factors of using a nonideal integrator has been studied in [17]. The frequency response of an integrator should reject DC bias and roll off quickly before reaching the system frequency range of interest to behave like an ideal integrator. Thus, the integrator is considered in the following form:

$$\frac{e_v}{e_a} = \frac{\tau_1 s}{(\tau_1 s + 1)(\tau_2 s + 1)} \tag{5.1}$$

where e_a and e_v denote acceleration and velocity signals, respectively. In this case, the following condition is used.

$$\tau_1 = \tau_2 = 10\sqrt{m_s/k_s} \tag{5.2}$$

Equation (5.2) indicates the integrator roll-off frequency point is one decade away from the body resonance point. Under the assumption of (5.2), this nonideal scheme usually affects the performance around 0.1 Hz. This fact can be seen from the performance of LQG-V and CGOF systems.

5.2 Evaluation of Performance Criteria

As LQG designs are done by the loop transfer recovery of LQR system, no matter what kind of feedback signal is used, the role of the observer is just to provide actuator with state estimate which is determined by the sensor's noise intensity μ. This explains why no significant difference is observed among the LQG performance results, as shown in Fig.6 & Fig.7. The average ride comfort improvement compared to passive system is about 5–8 dB, primarily in the range of [1 Hz–5 Hz]. This improvement substantially eliminates the body resonance in acceleration and tire deflection. The price paid with the above improvement is the elevated low frequency suspension deflection, depending on how far the ride comfort is achieved. At high frequency range, ride comfort improvement is achieved at the expanse of higher suspension and tire deflection. In the cases of CGOF and SPT, the ride comfort improvement show larger and wider band reduction than the ones of LQG systems, especially reaching further into wheel resonance region (see Fig.22 & Fig.23). The SPT [1 Hz–5 Hz] acceleration average reduction compared to passive is about 18 dB (see Fig.19).

In designing SPT controller, the closed loop high frequency damping is intentionally maintained the same as open loop; while in CGOF case, the controller gain K_c is tuned without affecting high frequency mode (see Fig.8 & Fig.9). Therefore, both CGOF and SPT will keep high frequency road holding ability and suspension deflection at least the same as the open loop system.

5.3 Controller Bandwidth and Force Level

The ride comfort improvement can be used, qualitatively, to reflect the bandwidth of the controller. The L.R.H. side of Fig.22 summarizes the controller frequency response from acceleration to force (Note that velocity is obtained by integrating acceleration). LQG-P is not shown in this plot because it uses a different measurement scheme from the other four systems. However, a fair comparison baseline is the force level requirement. Fig.23 & Fig.24 show the force level of all designs. Generally speaking, in low frequency range, SPT requires 10 dB more force level than LQG systems in [0.05 Hz–0.5 Hz], and has 10 dB less sprung mass acceleration in [0.5 Hz–5 Hz]; while at high frequency range, the LQG systems require higher force to maintain better damping; instead, SPT uses less amount of force to achieve better ride comfort. This fact is also true in the CGOF system.

5.4 Robustness Analysis

For the concern of robustness, the stability and performance of the feedback loop system $(C(s), G(s))$ should be maintained in the presence of model uncertainties including load, damping and tire stiffness variations, etc. In MIMO systems, assuming that the system model error can be characterized by multiplicative uncertainties, i.e.,

$$G(s) + \delta G(s) = [I + L(s)]G(s) \tag{5.3}$$

where L(s) is an arbitrary stable transfer function matrix with

$$\hat{\sigma}[L(jw)] \leq m(w) \tag{5.4}$$

the system's robustness can be measured by the widely used "complementary sensitivity function" [26, 27], as defined below:

$$T(s) = G(s)C(s)[I + G(s)C(s)]^{-1} \tag{5.5}$$

With $m(w)$ denoting the upper bound of normalized magnitude that the model error can tolerate, it is shown that stability is maintained in the presence of all possible uncertainties described by (5.3)–(5.4) if and only if

$$\hat{\sigma}[T(jw)] \leq \frac{1}{m(w)} \tag{5.6}$$

The $m(w)$ is typically small at low frequency but goes up to unity and above as frequency increases [2, 26].

In active suspension systems, $T(jw)$ is a scalar term. The singular value bode plot of various designs is shown in Fig.25 including SPT-2 design. It is easily seen that all of the acceleration measurement schemes, except LQG-P, have similar behavior. Without taking LQG-P into consideration, CGOF shows better robustness property than the others because its largest magnitude is kept at unity (which implies allowing 100% model error) and starts to roll off at 2 Hz. The unity level is also observed in SPT and SPT-2 designs, but their roll-off frequencies are at about 20 Hz and 30 Hz, respectively. This is reasonable because SPT (and SPT-2) the fast compensators $C_f(s)$ are intentionally introduced in high frequency range to achieve high frequency design goals. This high frequency dynamics does not exist in the CGOF design due to the velocity $\dot{z}_s$ (slow variable) feedback and the limited stabilizing range of the gain K_c. As for LQG-A and LQG-V, the singular value rises up to 8 dB around wheel resonance. Therefore, the allowable model error has to be limited to 40%.

As stated previously, $m(jw)$ is typically small in low frequency region. This might make LQG-P still acceptable in spite of its elevated DC value. At the frequency range above 1 Hz, it is always below unity and rolls off at 10 Hz. However, the relative advantage over the other systems can not be determined unless we can understand more characteristics about acceleration and position measurements schemes.

5.5 Performance Variation Due to Parameter Perturbation

Another approach of robustness analysis is to investigate the performance variations when parameters perturbation occur. The perturbation of 50% increase in damping coefficient (b_s) and 25.7% decrease in sprung mass (m_s) relative to nominal value have been investigated in [24]. For a real vehicle, the opposite perturbation also happens, but it is claimed that the change in this direction as stated above represents the worst case. We thus consider the above two cases in our analysis. Besides, the perturbation of tire stiffness, which plays an important role in high frequency dynamics, is also of interest. Due to modeling error or environmental influence, it is assumed that the tire stiffness could be varied from 50% decrease to 50% increase relative to its nominal value. This is equivalent to a 50%–150% wide variation range. For the sake of simplicity, the analysis is performed only on LQG-P, CGOF and SPT, representing different measurement schemes of position, velocity and acceleration, respectively.

5.5.1 Perturbation of 50% Damping (b_s) Increase

Fig.26, Fig.27, & Fig.28 show the damping perturbed performance, where the solid lines represent the nominal performance and the dashed lines represent the perturbed performance. This perturbation causes the three systems about 2–4 dB ride comfort degradation in [1 Hz–10 Hz]. A little bit loss in road holding ability is also noticed. As for suspension deflection, the influence is not significant. In general, the three systems have comparable robustness property to damping perturbation.

5.5.2 Perturbation of 25.7% Sprung Mass (m_s) Decrease

The vehicle load fluctuates quite often, and is usually characterized by sprung mass variation. The assumption of 25.7% decrease results in 1–3 dB ride comfort loss in the three systems, while requiring less suspension and tire deflection, as shown in Fig.29, Fig.30, & Fig.31. Likewise, the solid lines represent the nominal performance and the dashed lines represent the perturbed performance. In fact, SPT sprung mass acceleration is more insensitive to mass variation except at the wheel resonance point. This property is not considered as relatively important because the other two systems are still quite comparable.

5.5.3 Perturbation of ±50% Tire Stiffness (k_t)

Next, a wide range, from 50% decrease to 50% increase, of tire stiffness is assumed. The results are demonstrated in Fig.32, Fig.33, & Fig.34. Clearly, all of their wheel resonances are shifted lower or higher, and their performance band variations appear without any significant difference. No relative advantage is offered by any system. This fact shows that tire stiffness change has similar influence on each system.

On the other hand, if we investigate the perturbational influence on the three performance criteria, it might be concluded that the increase of tire stiffness causes (1) deprivation of ride comfort, (2) requirement of larger working space, (3) loss of road holding ability. For the case of ride comfort, it can be considered as better if only the range of [1 Hz–10 Hz] is concerned, which is claimed in [24] as the main sensitivity region of human being[1]. But for road holding ability, it is not sufficient to look at only tire deflection when tire stiffness is perturbed, because the road holding is measured by the contact force fluctuation between the tire and road surface as stated in Section 1.4. Thus, a much worse road holding comes out. For more references about this issue, please refer to [11].

[1]Actually, the region is claimed as [3 Hz–8 Hz] in [24].

Chapter 6

Conclusions

The potential of using acceleration feedback has been explored in this thesis. It is shown that ride comfort can be improved over a wider frequency band, reaching into the wheel resonance. The improved design is achieved via characterizing the dynamics into slow and fast models and designing compensators individually to meet desired specifications for low and high frequency ranges. The design takes advantage of a more general use of acceleration feedback, compared with the more typical limited use when acceleration is integrated to produce velocity. The ride comfort improvement reported in [24] using "frequency weighted output feedback" is 8.3 dB at 20 rad/sec. ($\approx$ 3 Hz); and in [12] using LQG-P is the elimination of the sprung mass resonance. Here, the average band reduction on the frequency range of [1 Hz–5 Hz] is about 18 dB compared with the passive system, while still satisfying other performance concerns. A simpler scheme like CGOF might be attractive if acceleration integration is done properly. However, compared with the original passive system, the price paid for these achievements is the requirement of larger working space and some loss of road holding ability at the wheel resonance.

Another advantage of applying the two-time-scale technique to ASS is that the complexity of design task will be reduced a lot when we move up to solve a *full-car* problem. By the assumption of full car symmetry (see [2] for a full car model description), the original 14^{th} order full model can be decomposed into a 6^{th} order slow model (body) and four identical 2^{nd} order fast models (4 wheels).

m_s : sprung mass
m_u : unsprung mass
b_s : suspension damping constant
k_s : suspension spring constant
k_t : tyre spring constant
z_r : road displacement
u : control force

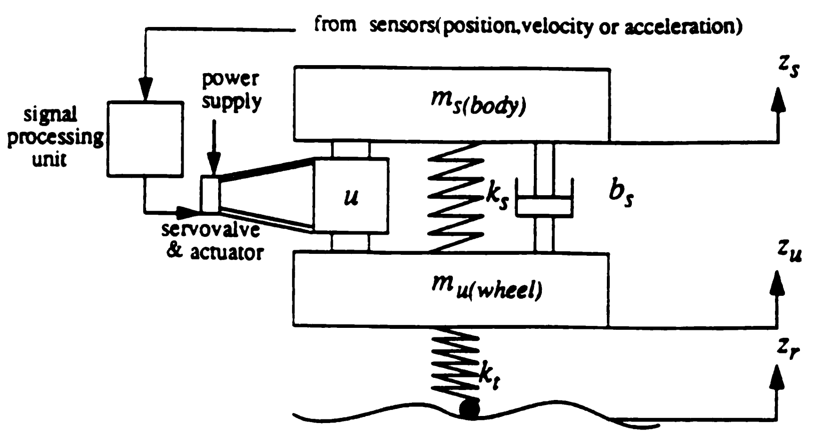

Figure 1: Structure of an Active Suspension System

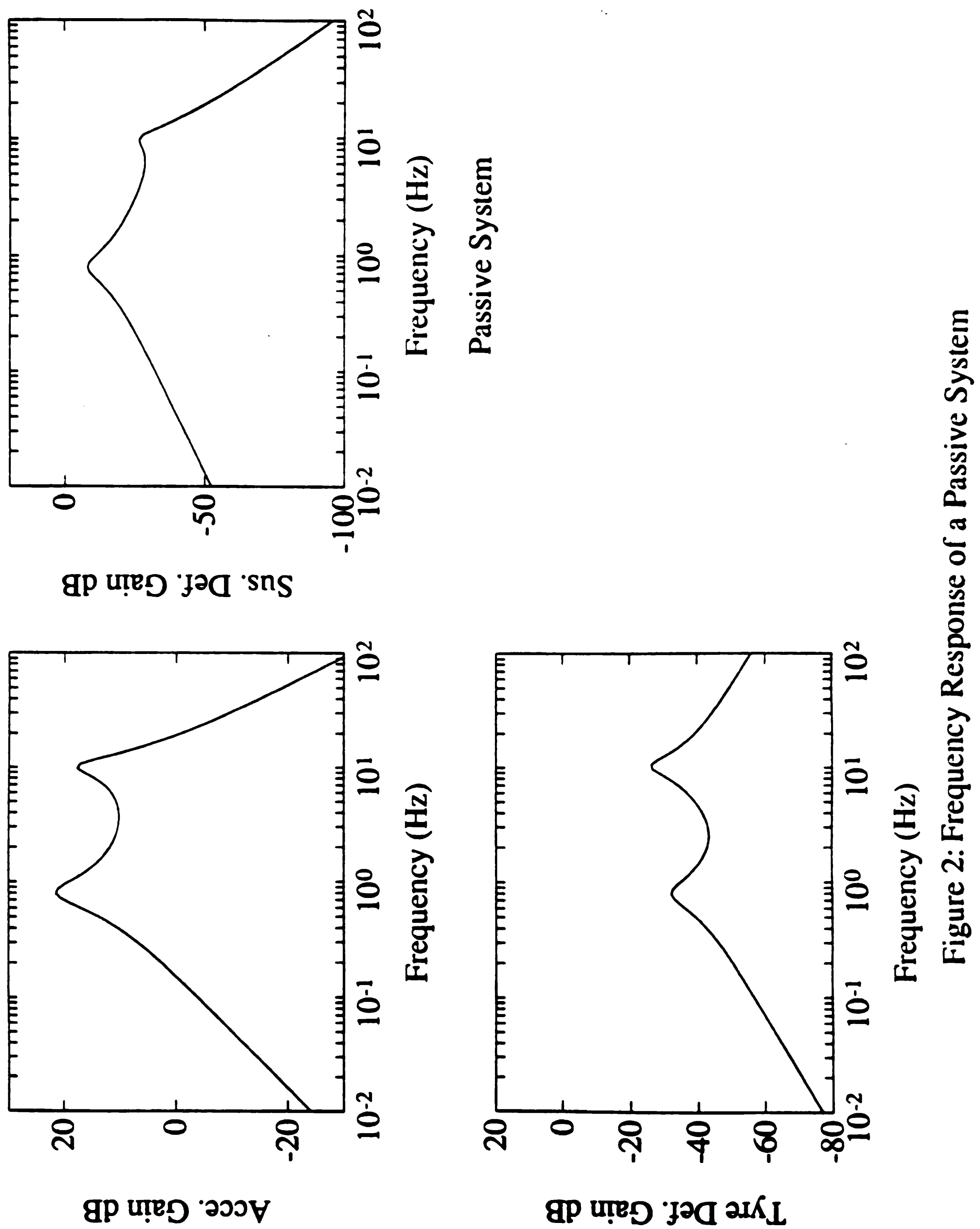

Figure 2: Frequency Response of a Passive System

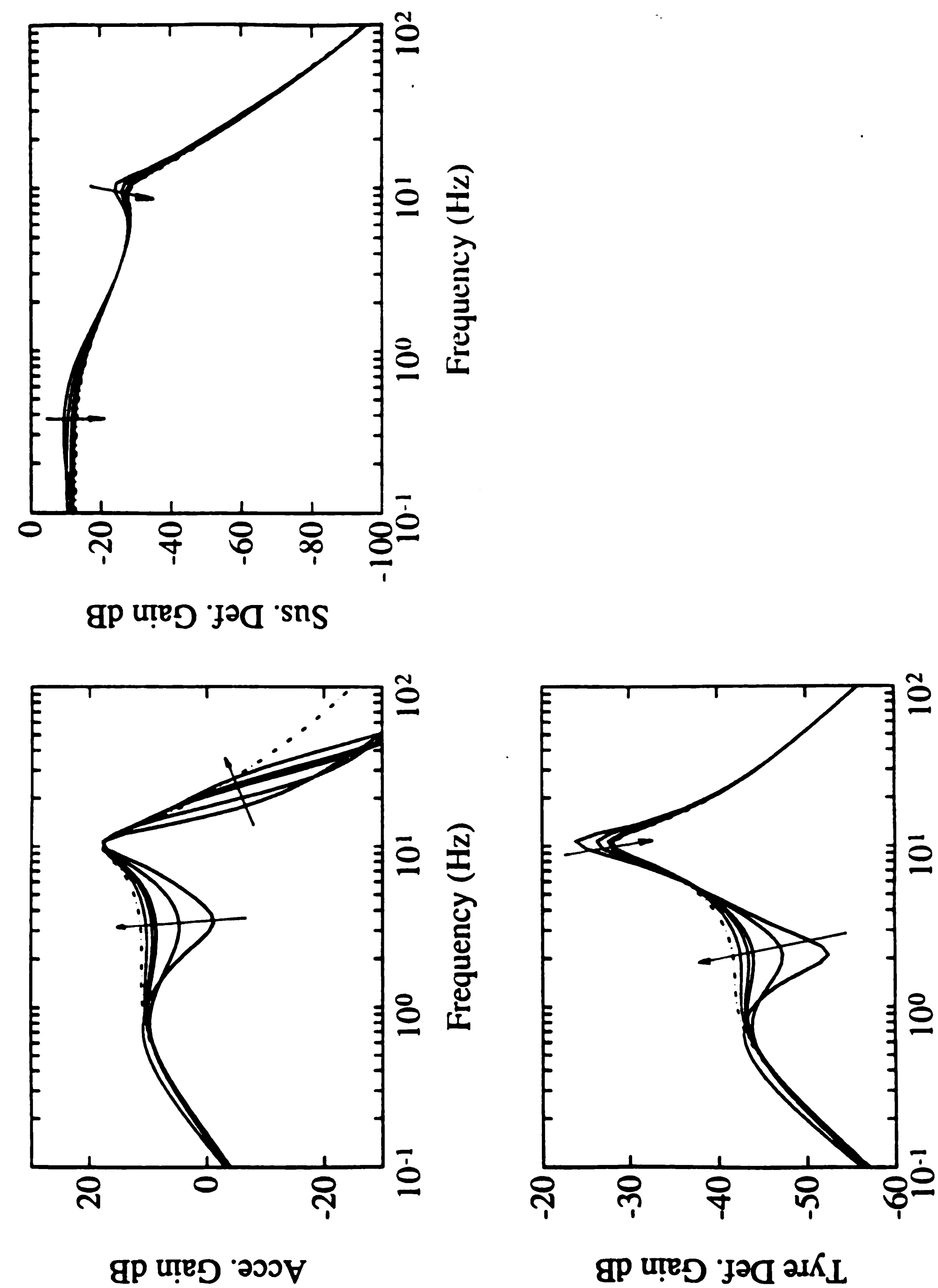

Figure 3: LTR of LQG-P System

Figure 3: LTR of LQG-P System

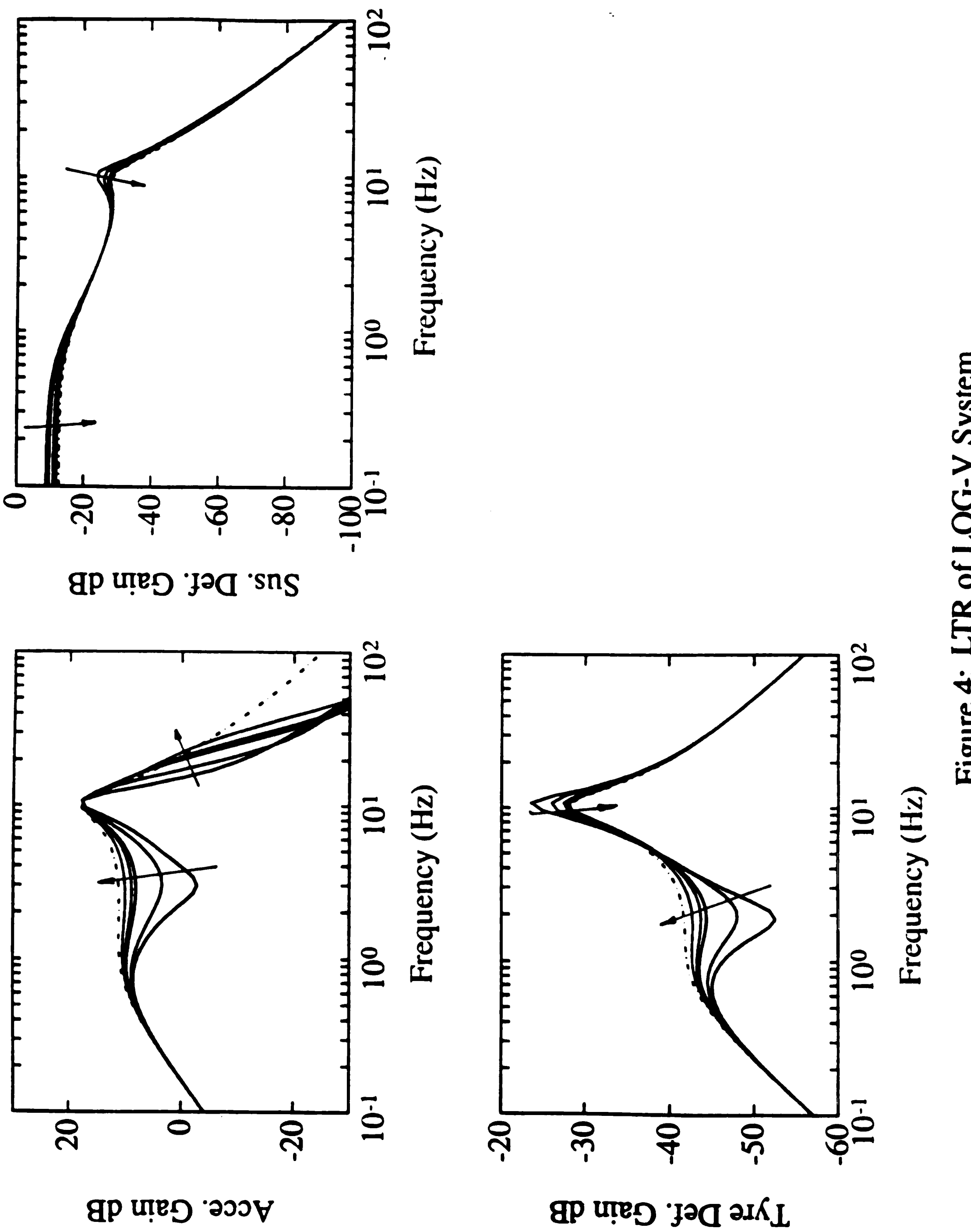

Figure 4: LTR of LQG-V System

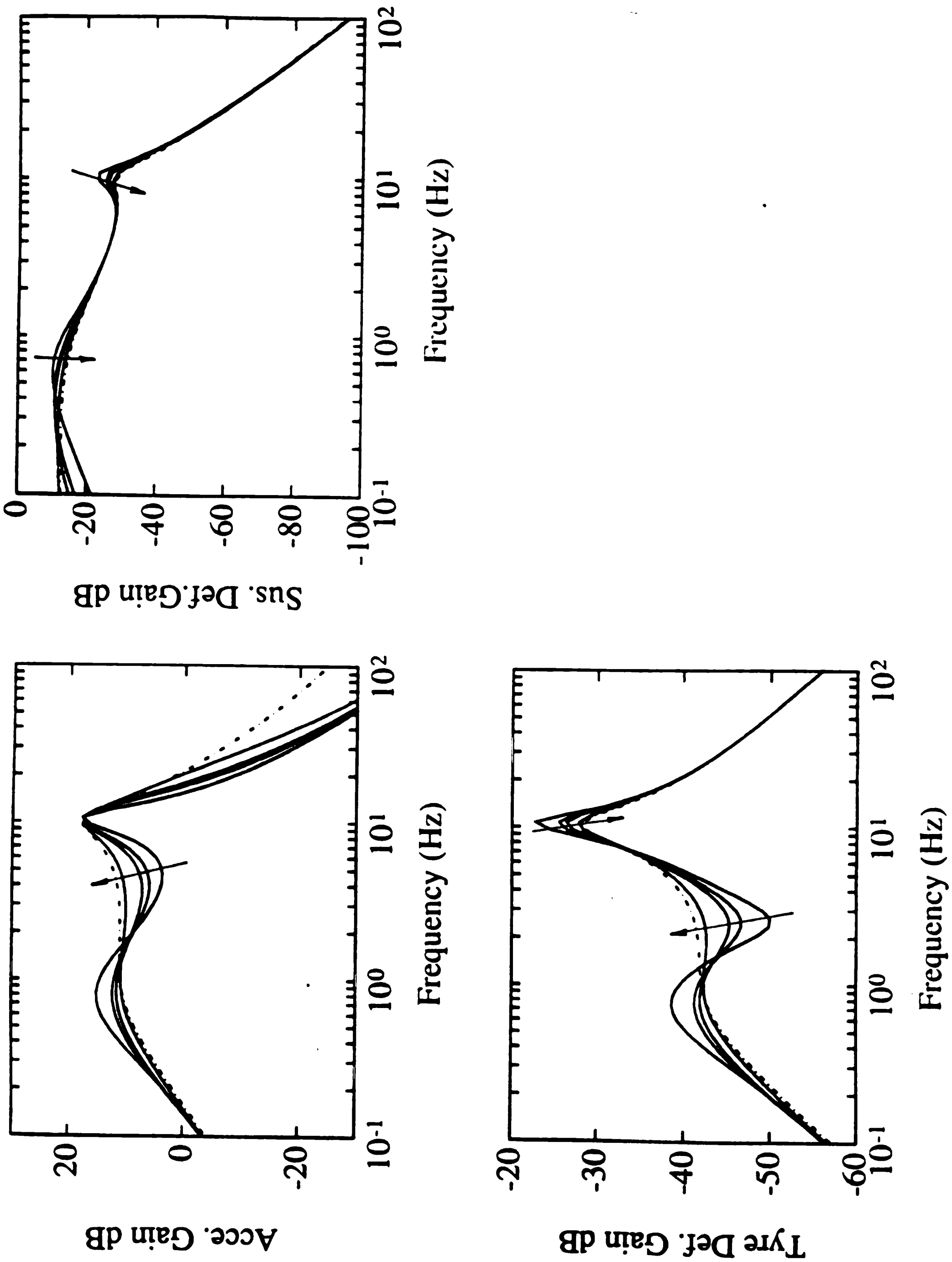

Figure 5: LTR of LQG-A System

Figure 5: LTR of LQG-A System

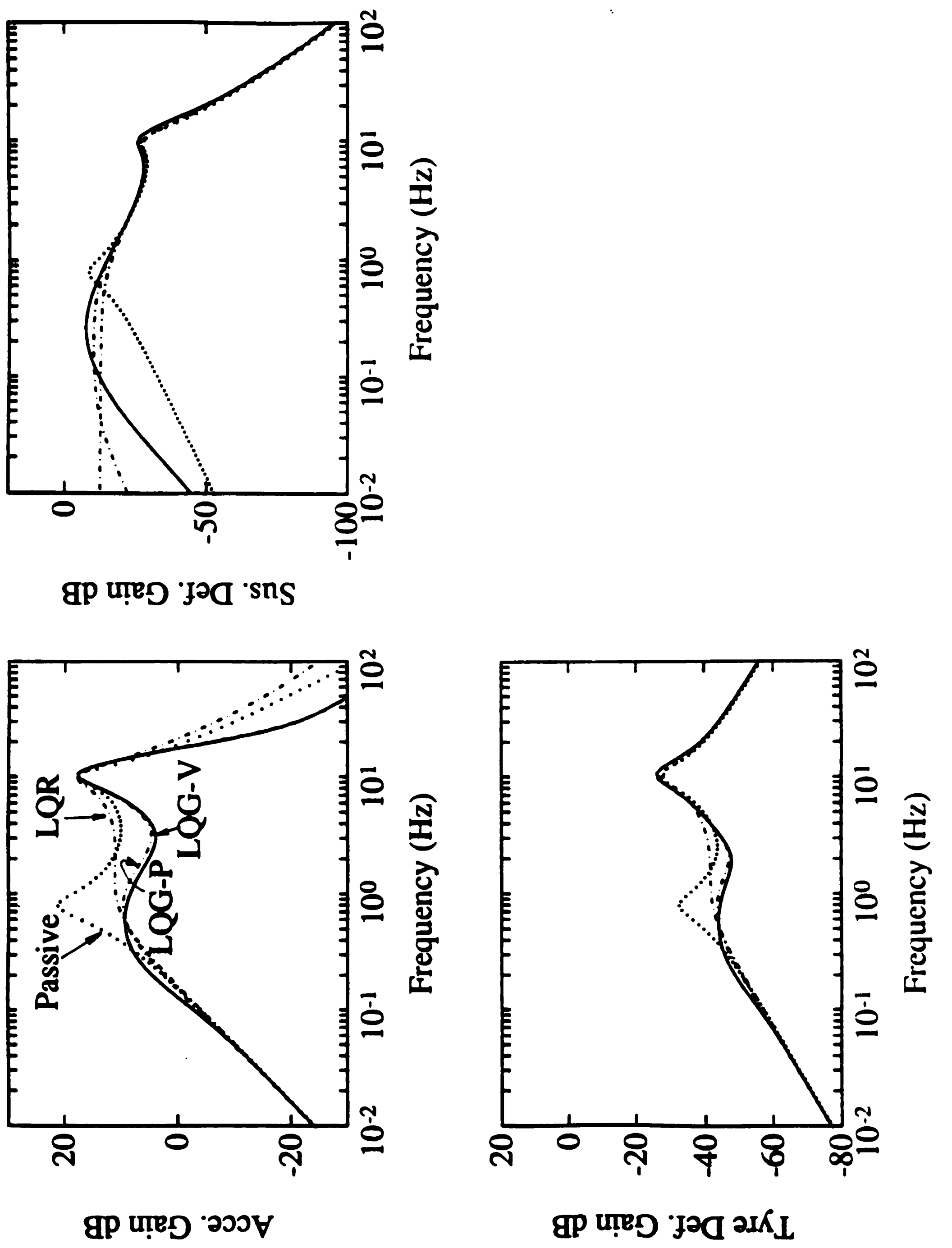

Figure 6: Performance of Passive, LQR, LQG-P & LQG-V Systems

Figure 6: Performance of Passive, LQR, LQG-P & LQG-V Systems

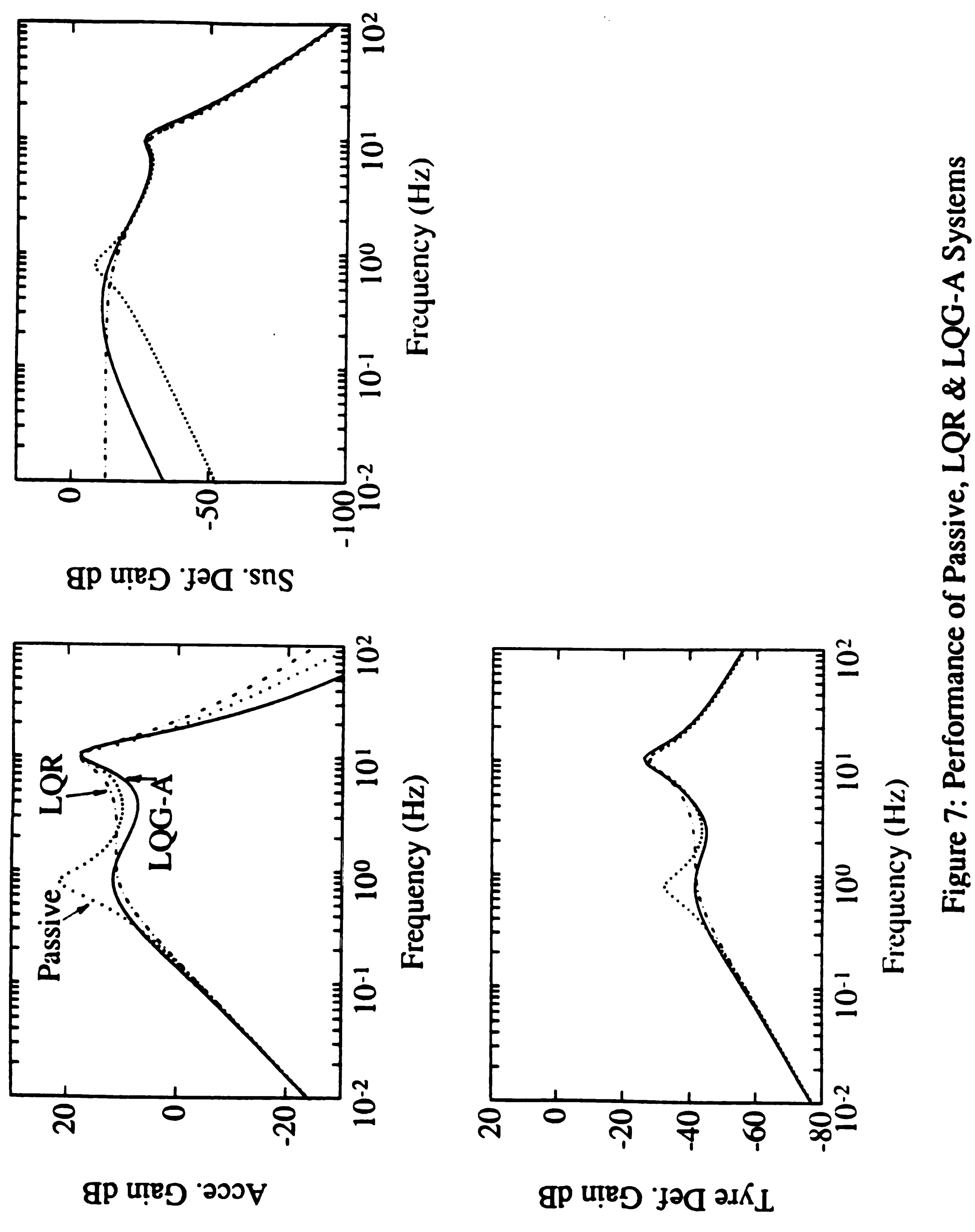

Figure 7: Performance of Passive, LQR, & LQG-A Systems

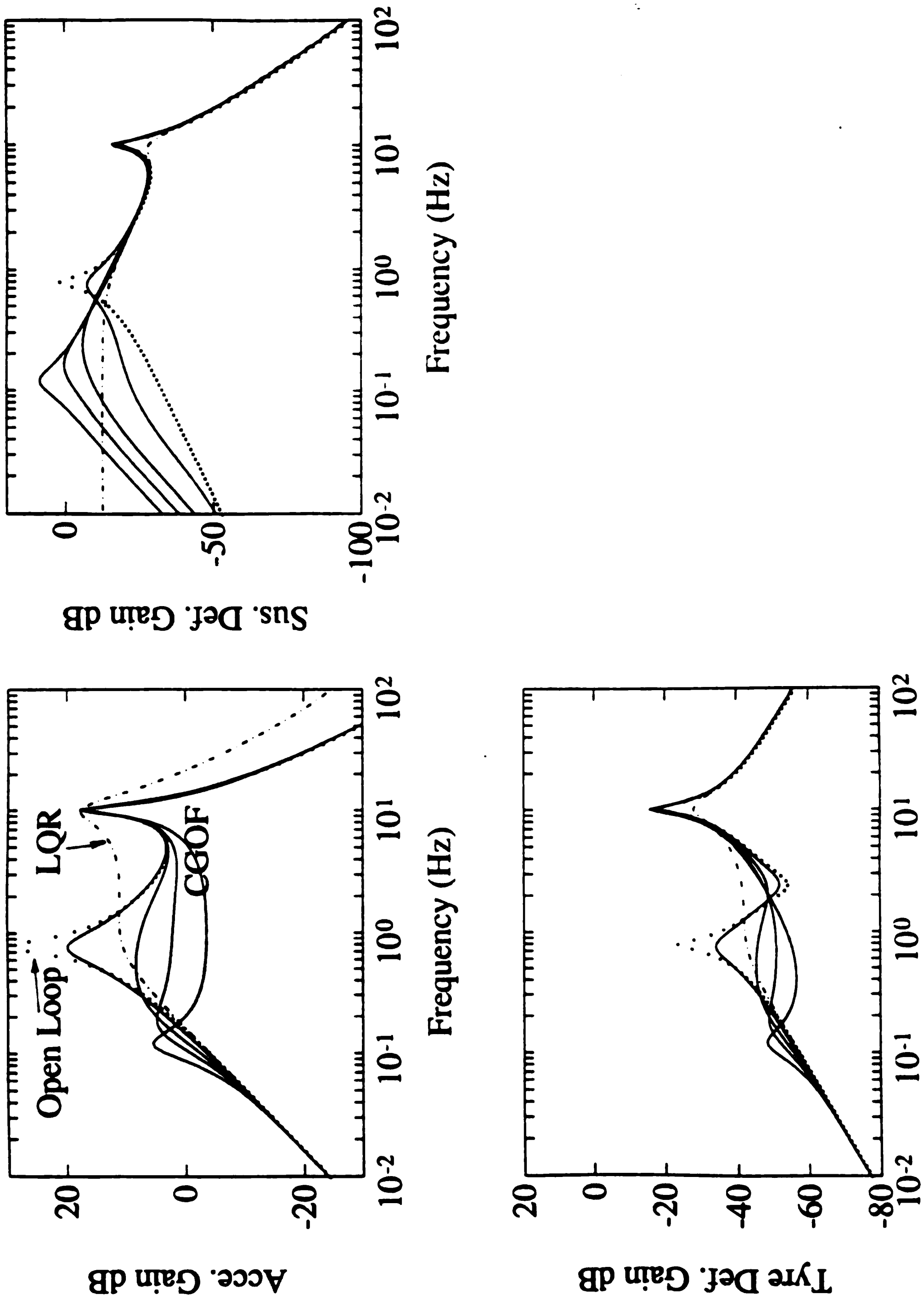

Figure 8: Design of CGOF (Velocity Feedback) System

Figure 8: Design of CGOF (Velocity Feedback) System

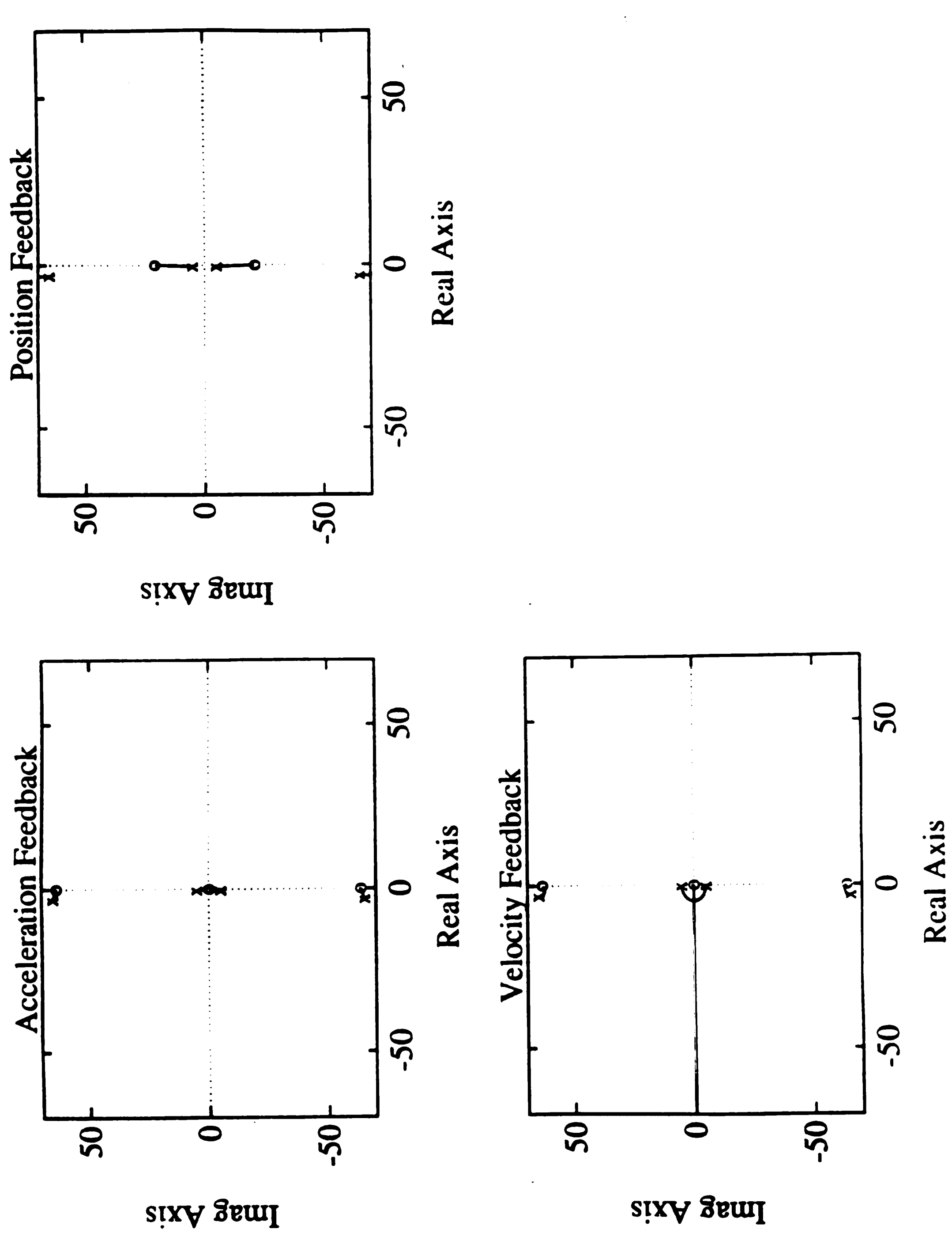

Figure 9: Root Locus of CGOF Systems (Position, Velocity & Acceleration Feedback)

Figure 9: Root Locus of CGOF Systems (Position, Velocity & Acceleration Feedback)

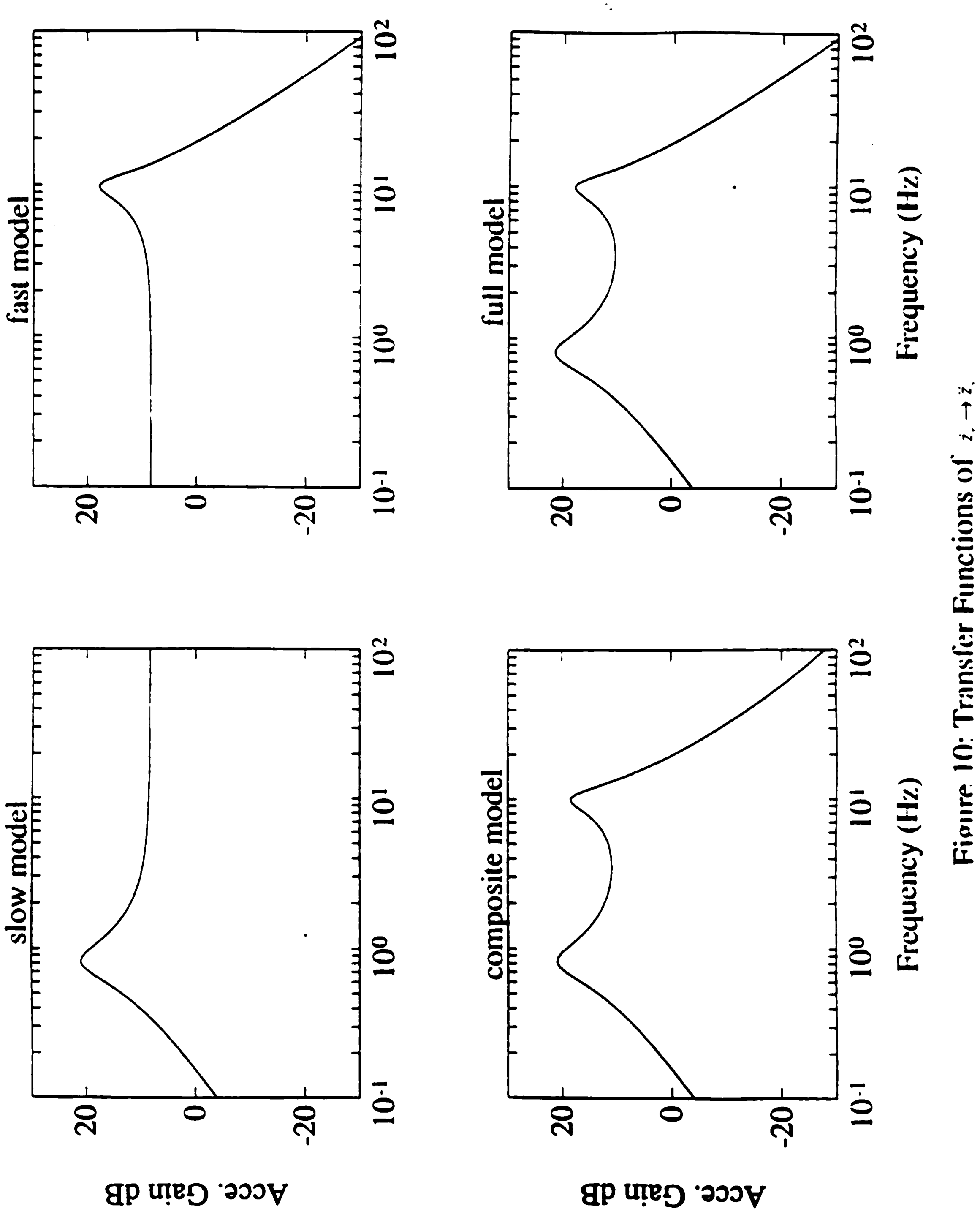

Figure 10: Transfer Functions of $\dot{z}_r \rightarrow \ddot{z}_s$

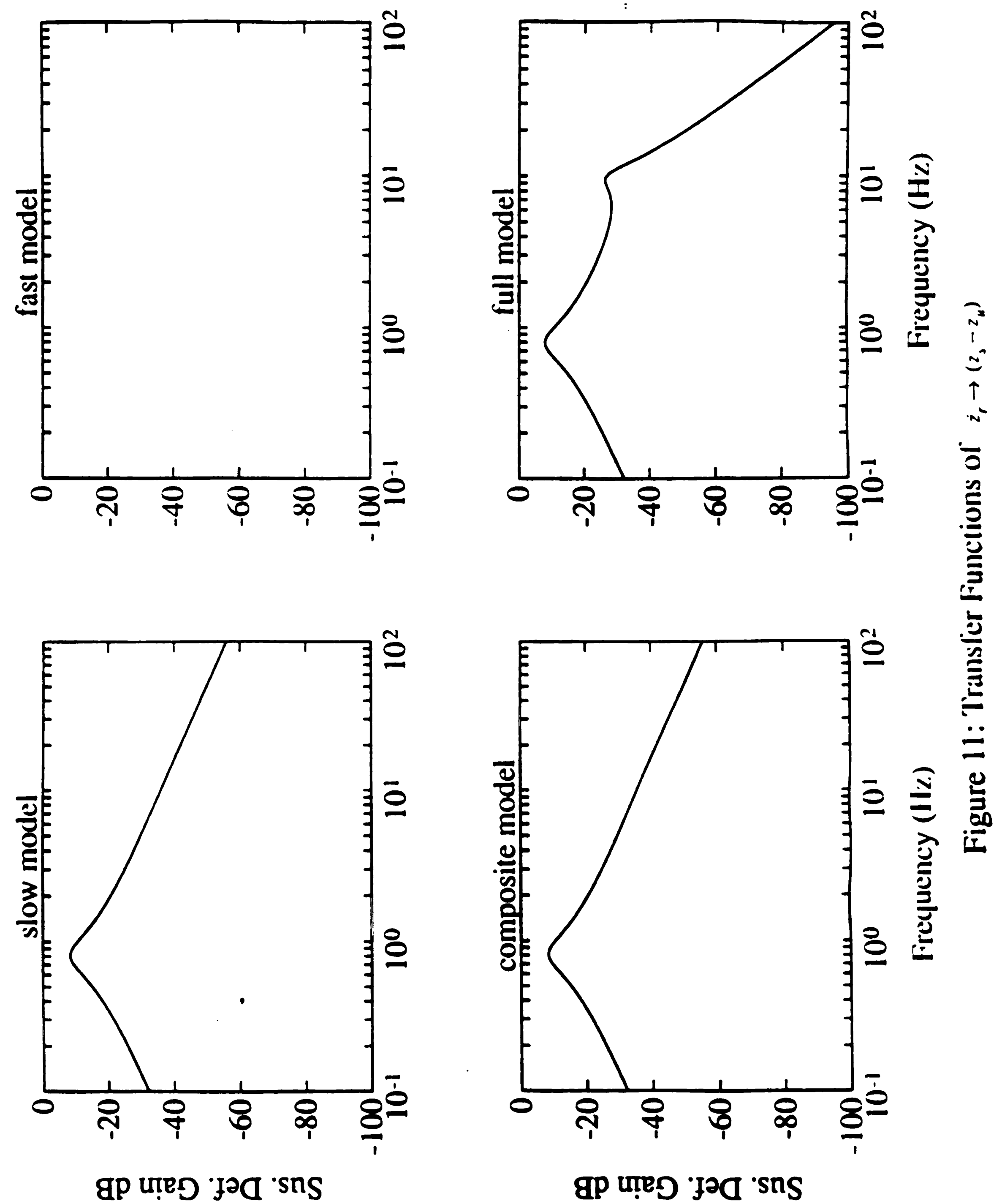

Figure 11: Transfer Functions of $\dot{z}_r \rightarrow (z_s - z_u)$

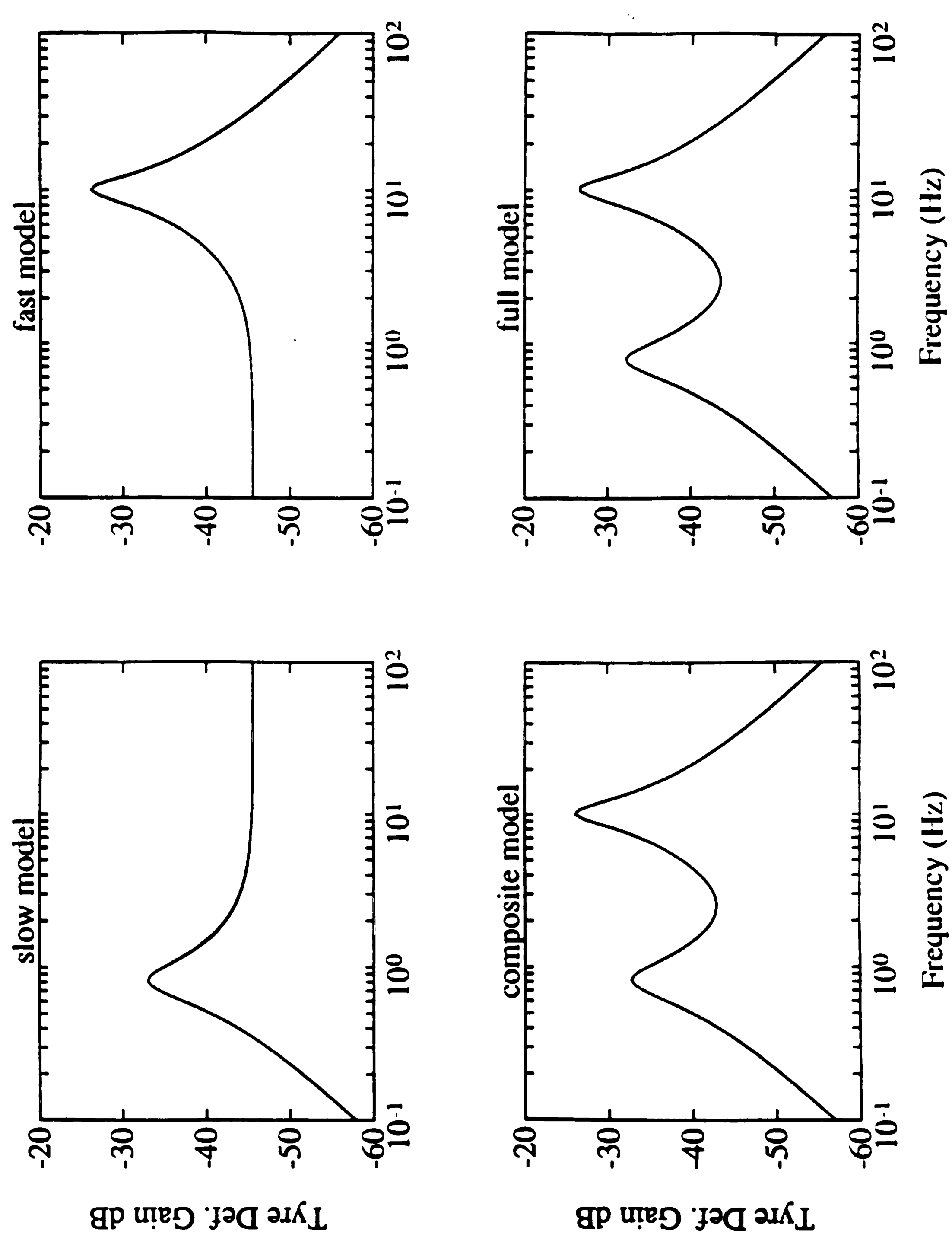

Figure 12: Transfer Functions of $\dot{z}_r \rightarrow (z_u - z_r)$

Figure 12: Transfer Functions of $\dot{z}_r \rightarrow (z_u - z_r)$

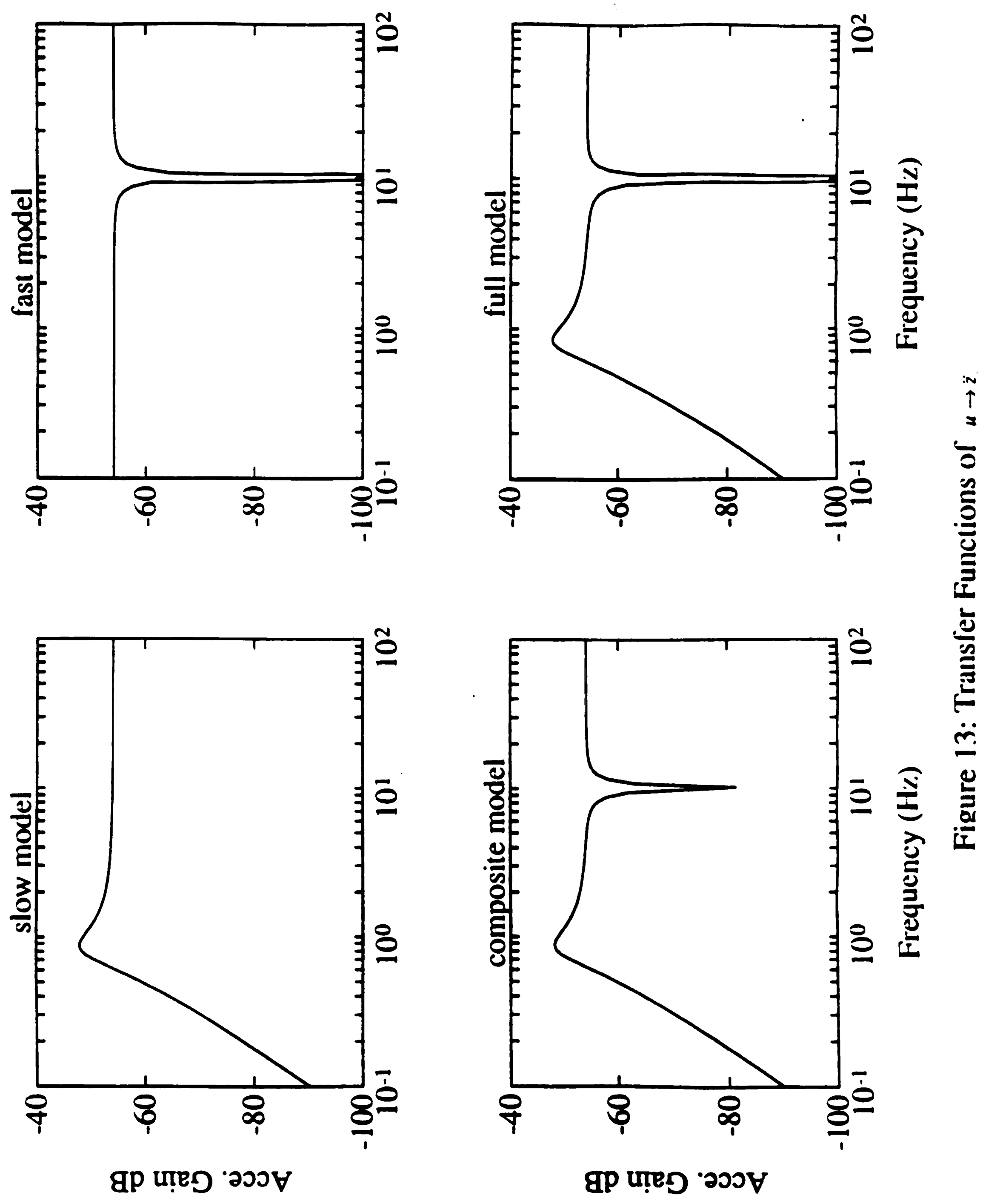

Figure 13: Transfer Functions of $u \to \ddot{z}_s$

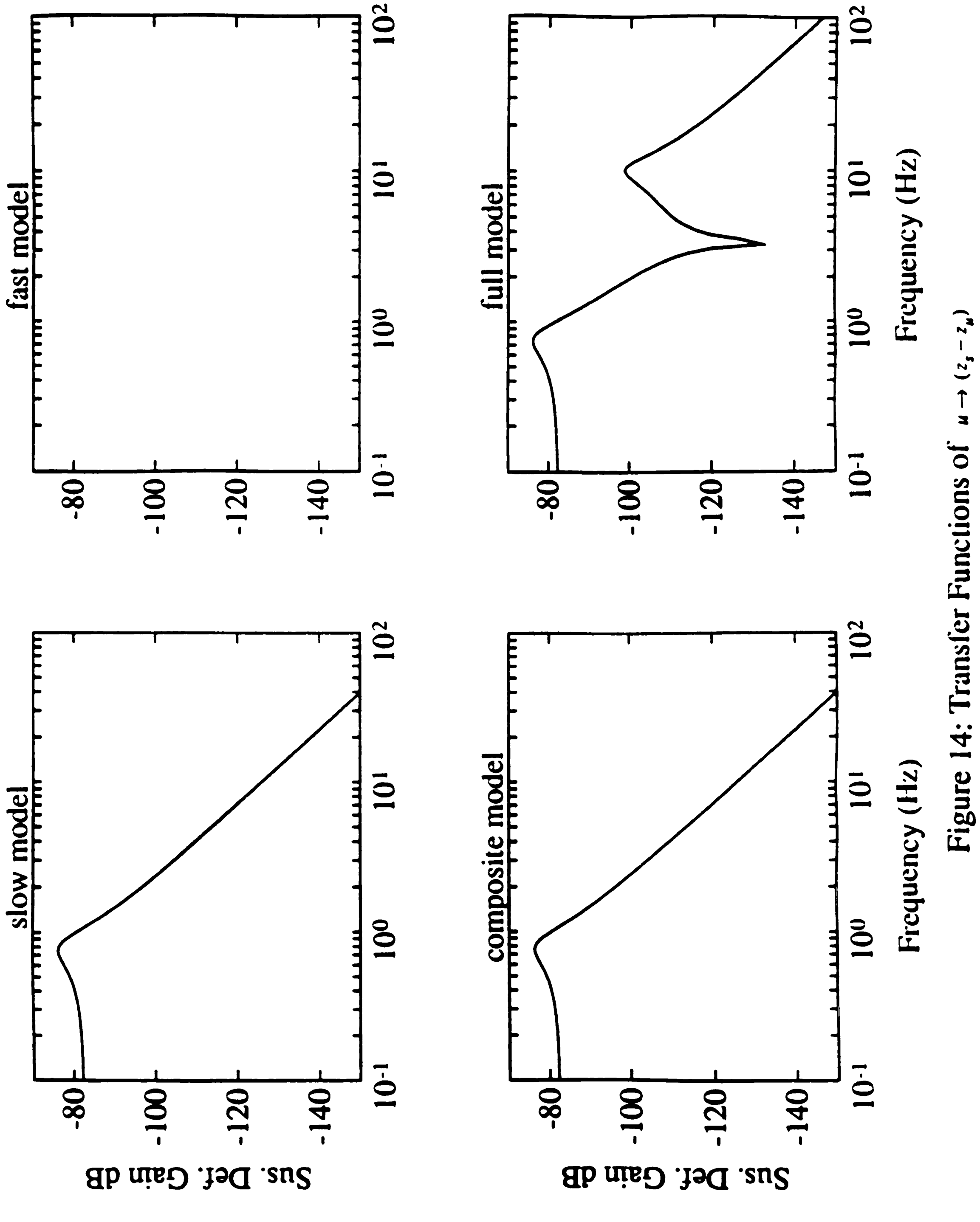

Figure 14: Transfer Functions of $u \longrightarrow (z_s - z_u)$

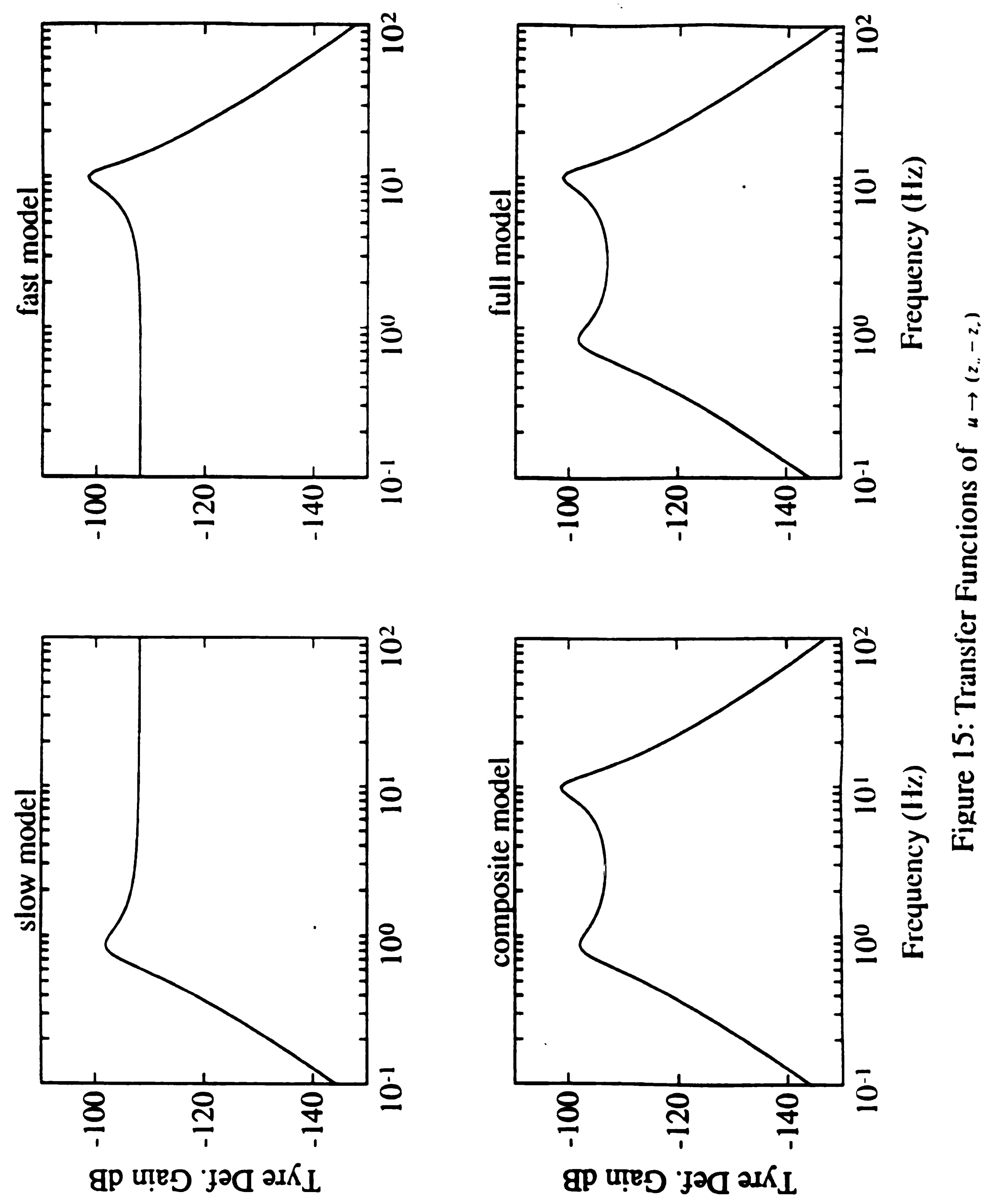

Figure 15: Transfer Functions of $u \rightarrow (z_u - z_r)$

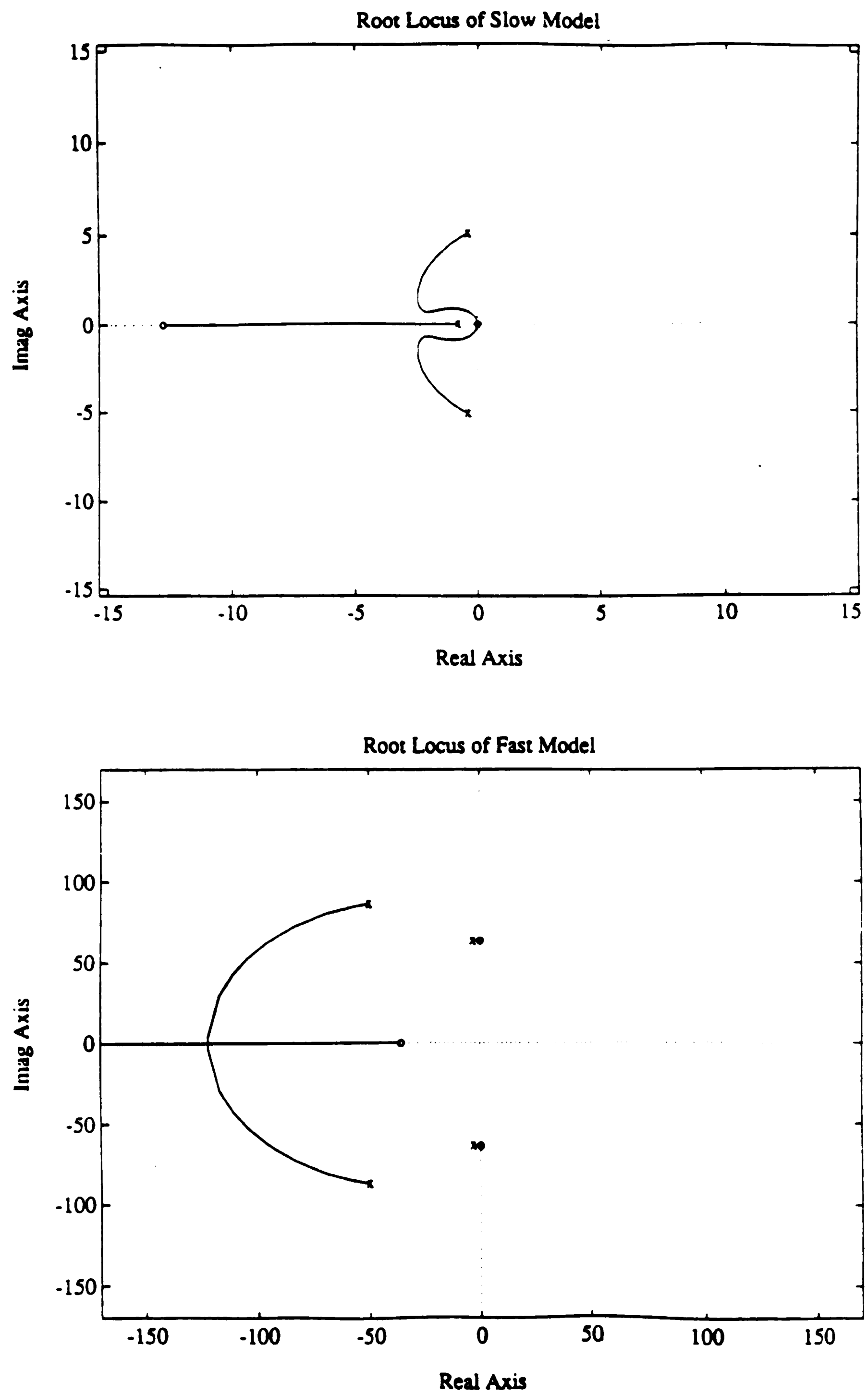

Figure 16: Root Locus of Slow and Fast Models (SPT-2)

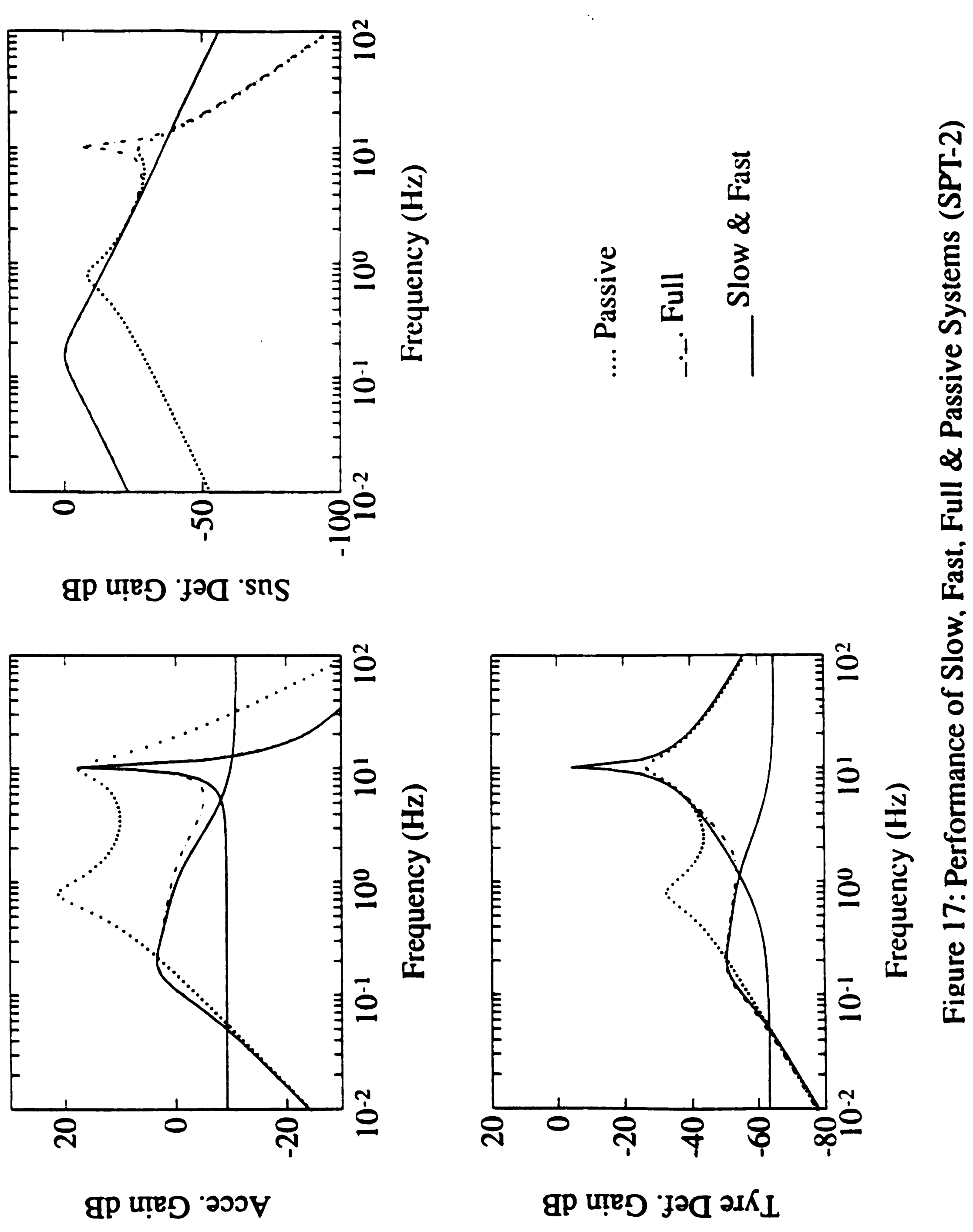

Figure 17: Performance of Slow, Fast, Full & Passive Systems (SPT-2)

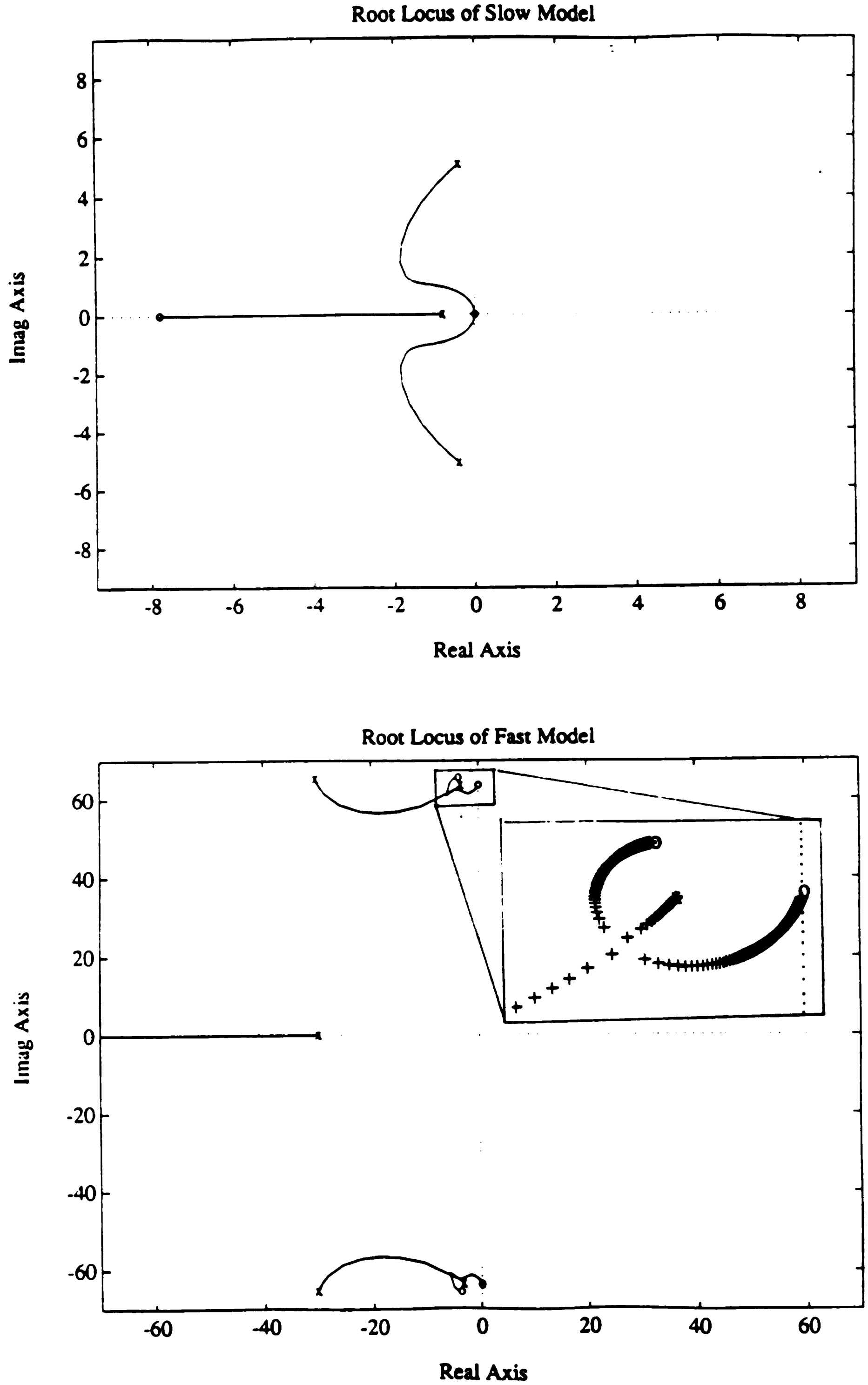

Figure 18: Root Locus of Slow and Fast Models (SPT)

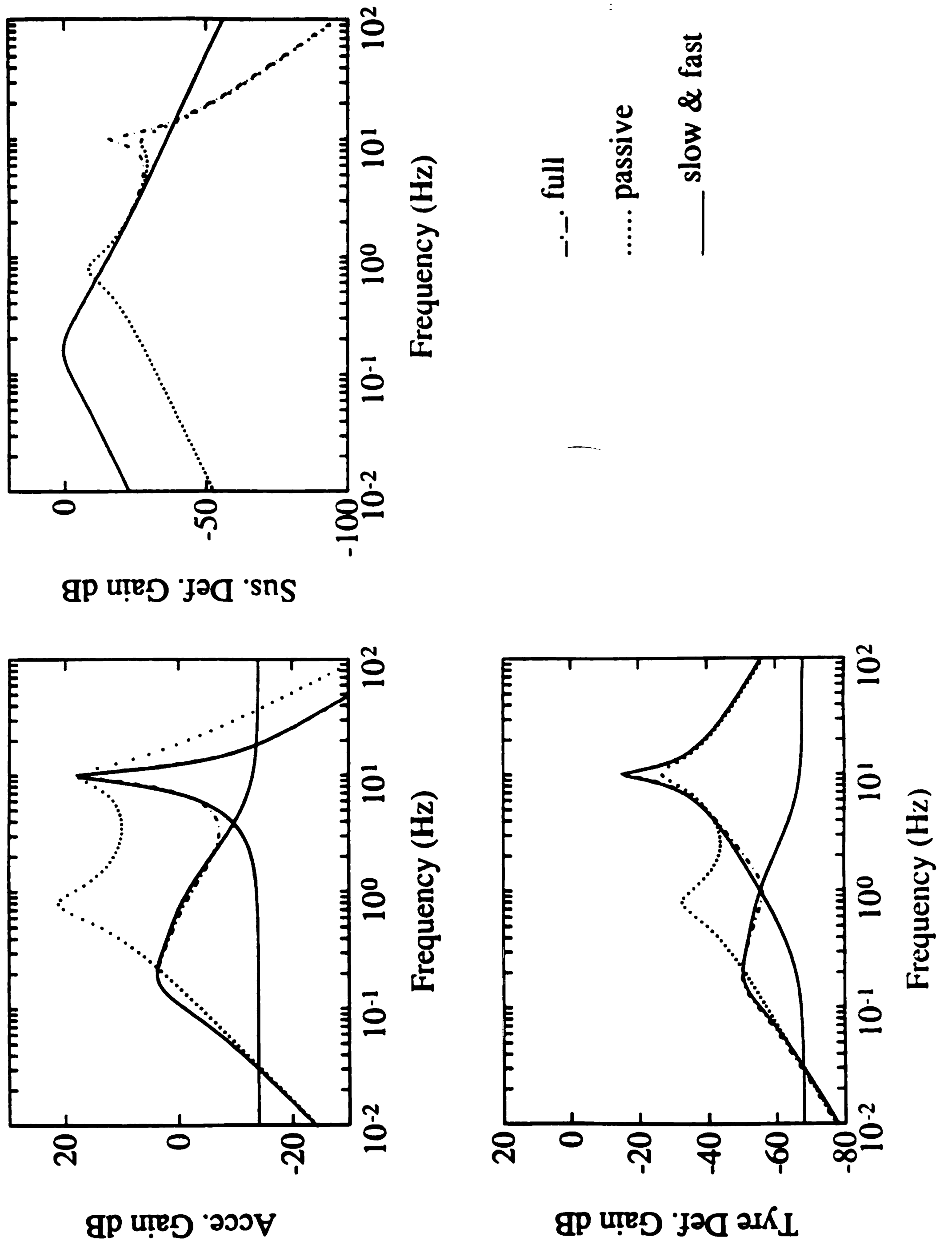

Figure 19: Performance of Slow, Fast, Full & Passive Systems (SPT)

Figure 19: Performance of Slow, Fast, Full & Passive Systems (SPT)

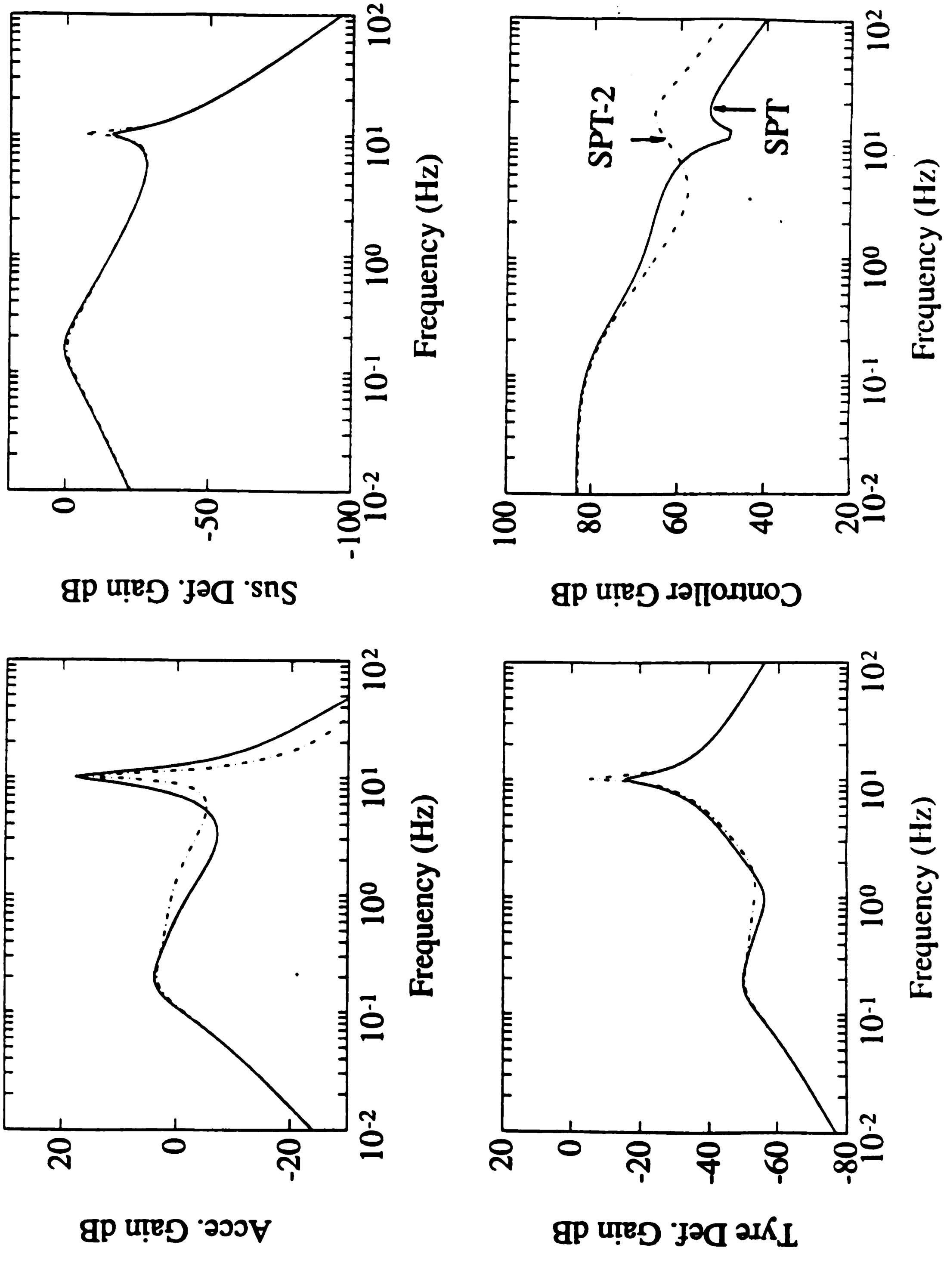

Figure 20: Performance & Controller Gain ($\dot{z}_r \rightarrow u$) of SPT & SPT-2

Figure 20: Performance and Controller Gain ($\ddot{z}_s \rightarrow u$) of SPT & SPT-2

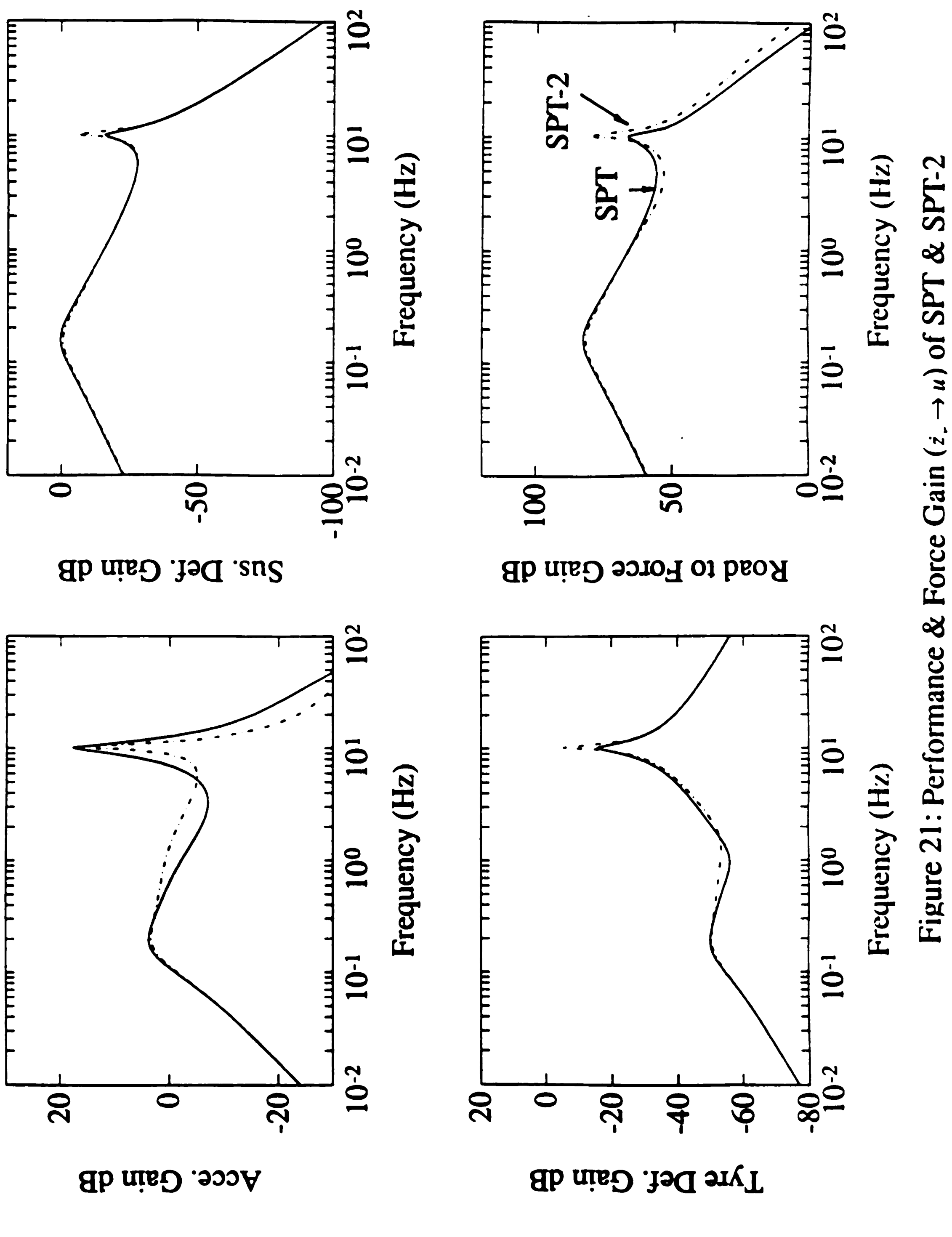

Figure 21: Performance and Force Gain ($\dot{z}_r \to u$) of SPT & SPT-2

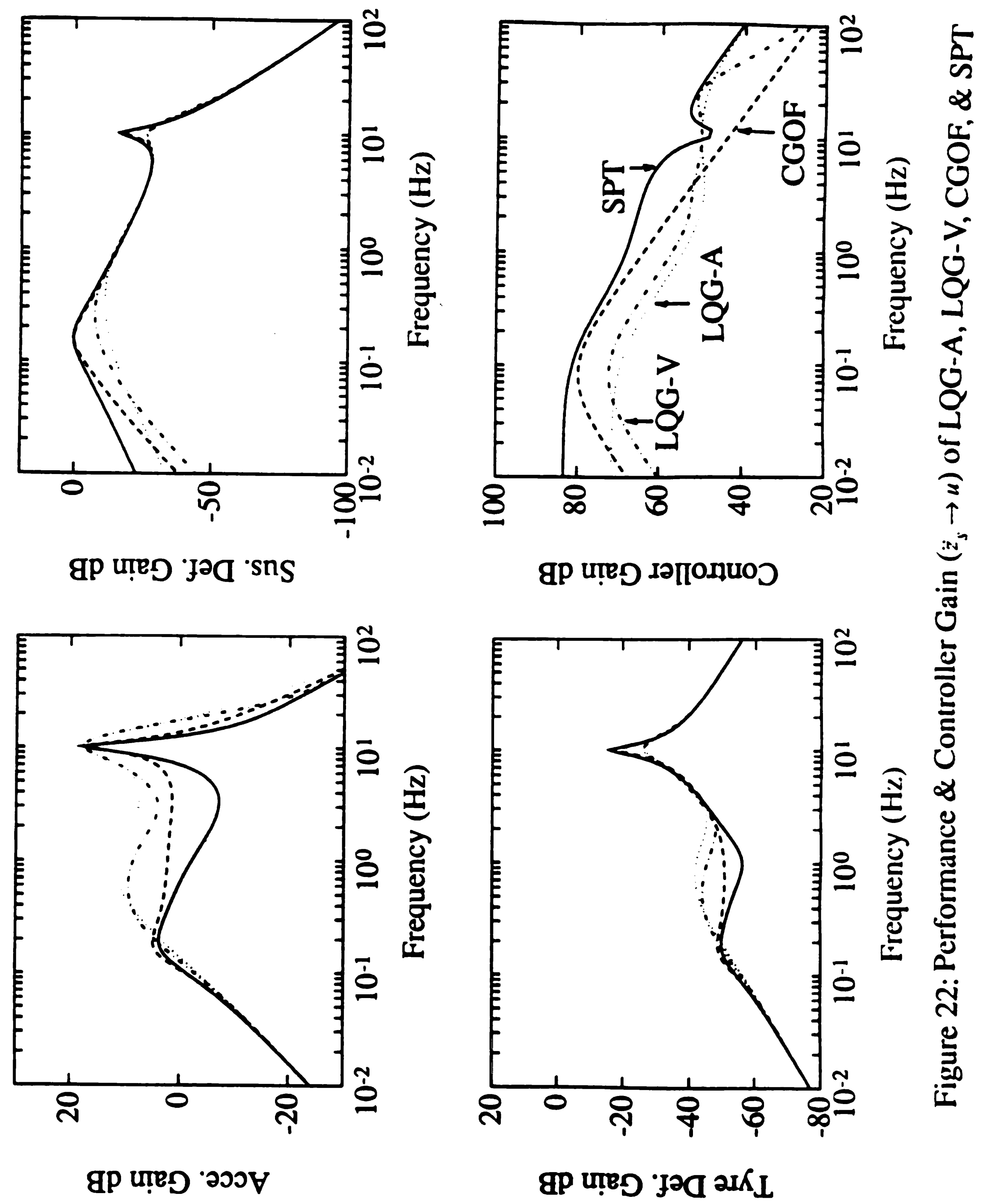

Figure 22: Performance and Controller Gain($\ddot{z}_s \rightarrow u$) of LQG-A, LQG-V, CGOF & SPT

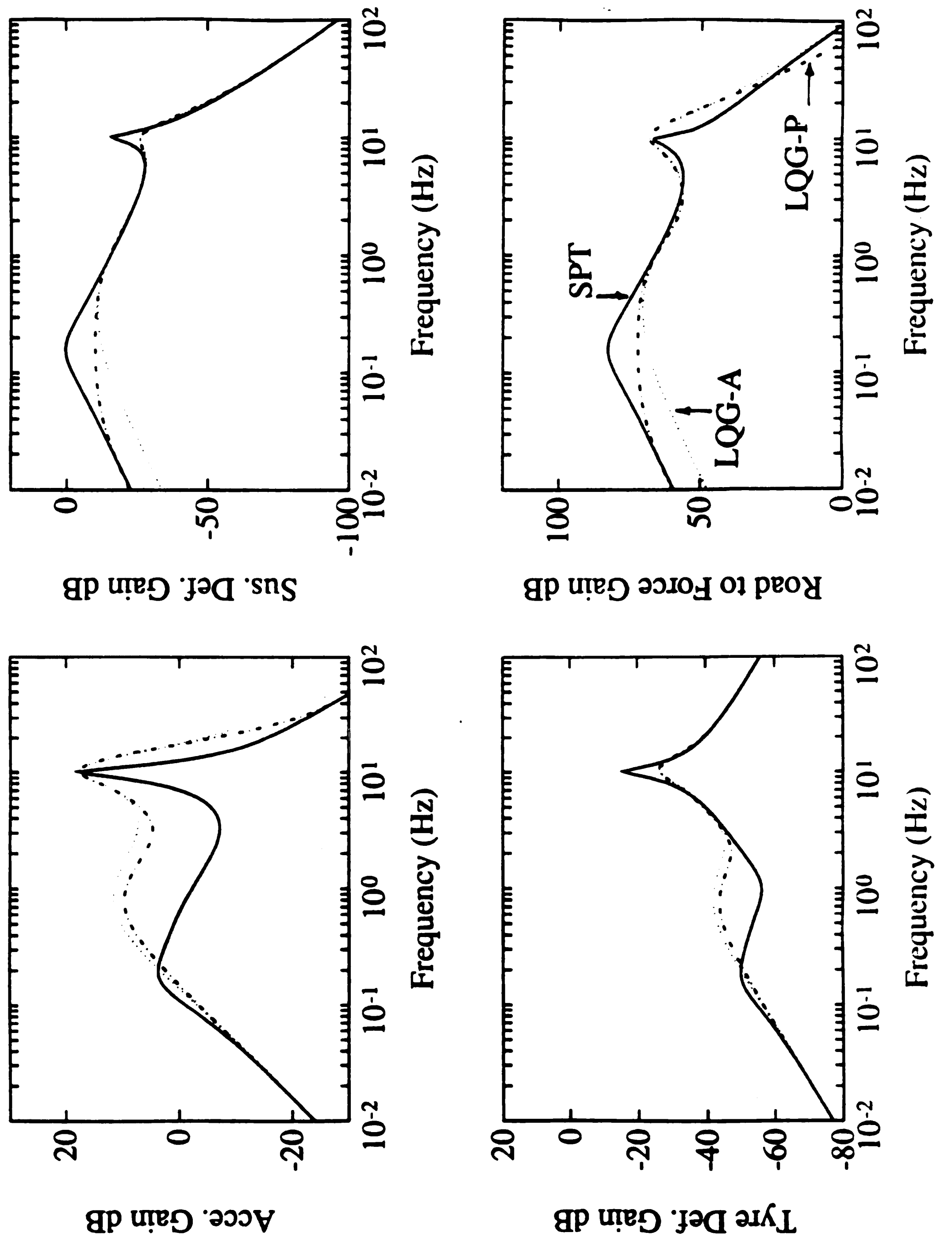

Figure 23: Performance & Force Gain ($\dot{z}_r \rightarrow u$) of LQG-A, LQG-P & SPT

Figure 23: Performance & Force Gain ($\dot{z}_r \rightarrow u$) of LQG-A, LQG-P & SPT

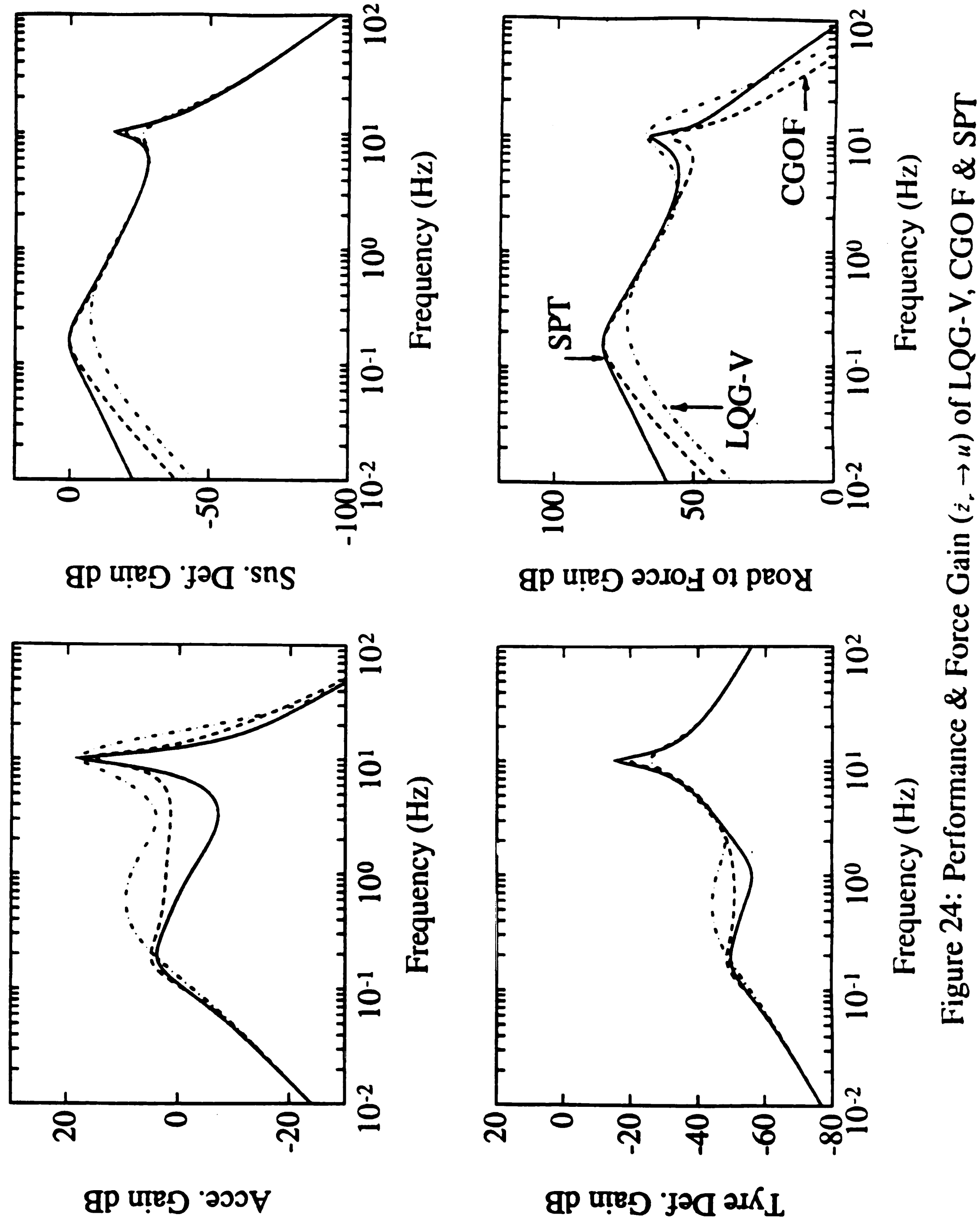

Figure 24: Performance & Force Gain ($\dot{z}_r \rightarrow u$) of LQG-V, CGOF & SPT

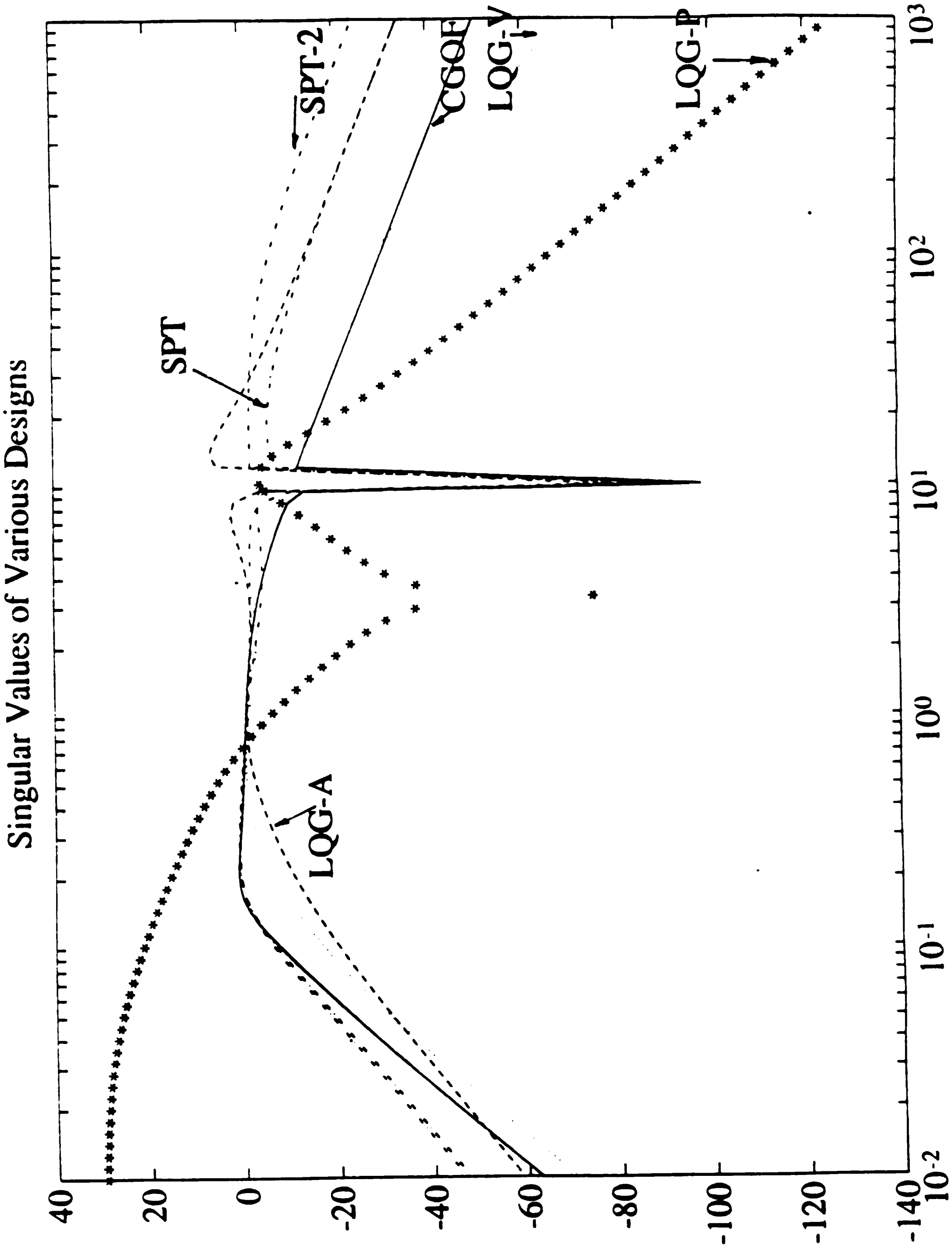

Figure 25: Singular Value of Various Designs

Figure 25: Singular Value of Various Designs

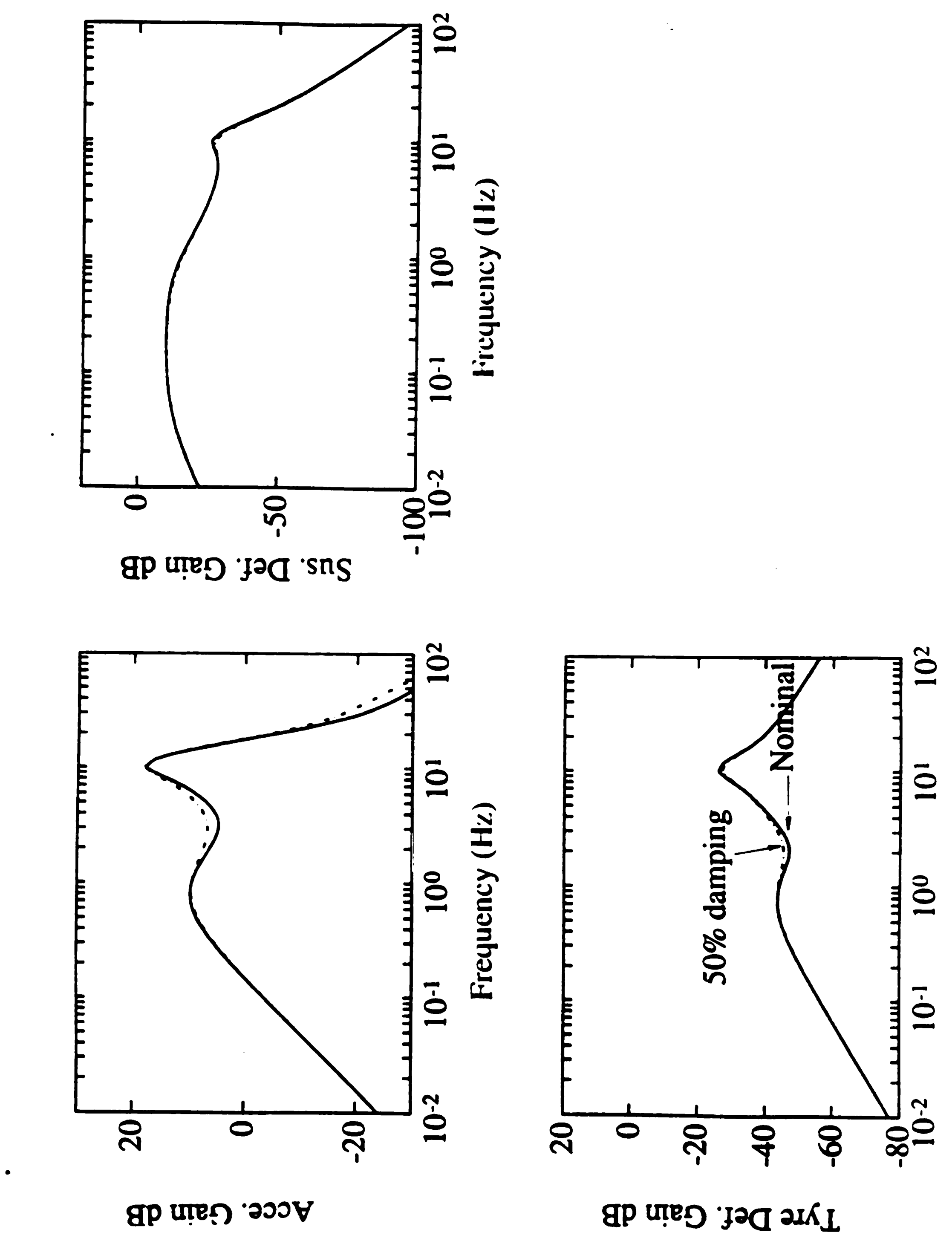

Figure 26: Performance of 50% Damping (bs) Perturbed LQG-P System

Figure 26: Performance of 50% Damping (b_s) Perturbed LQG-P System

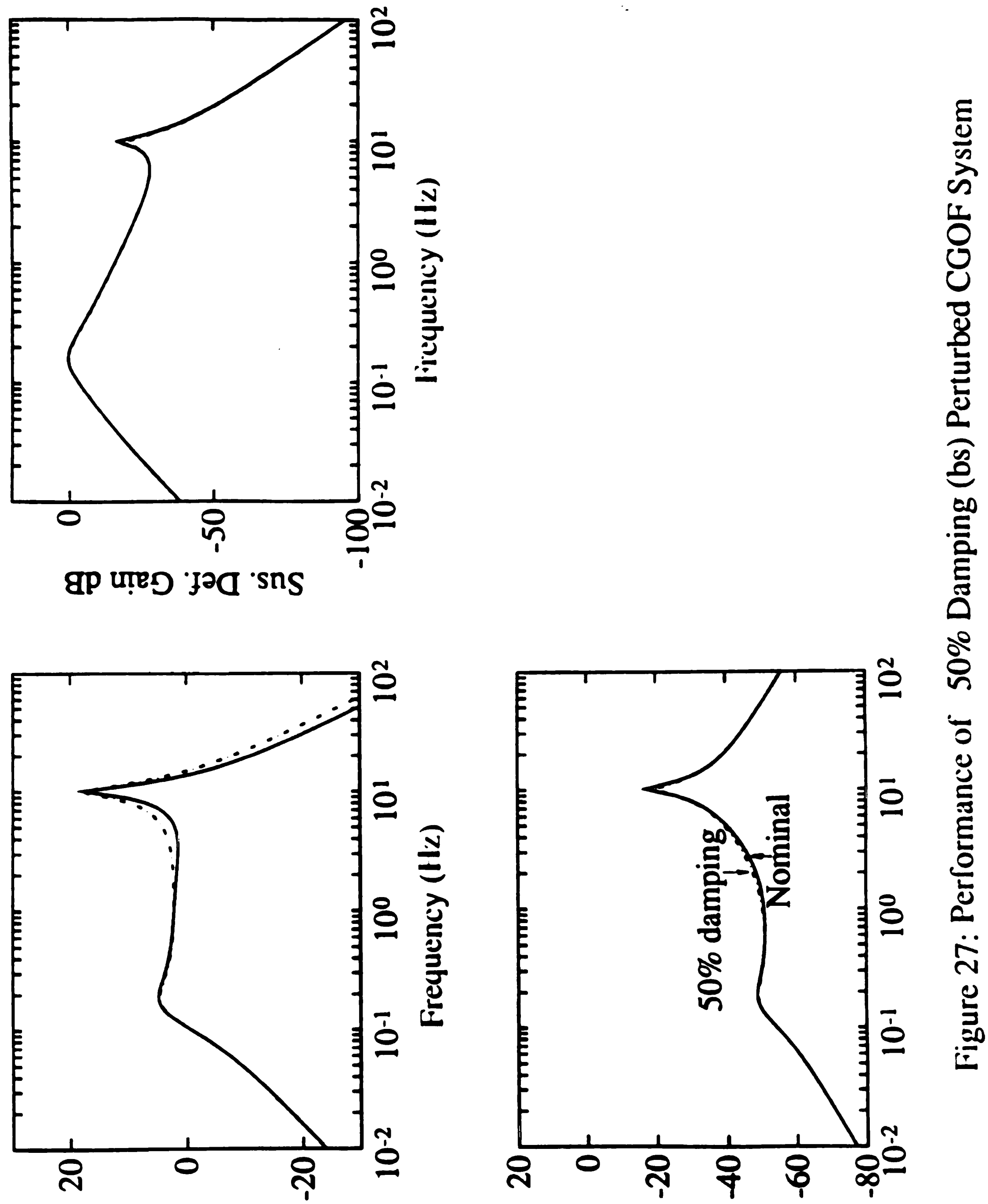

Figure 27: Performance of 50% Damping (b_s) Perturbed CGOF System

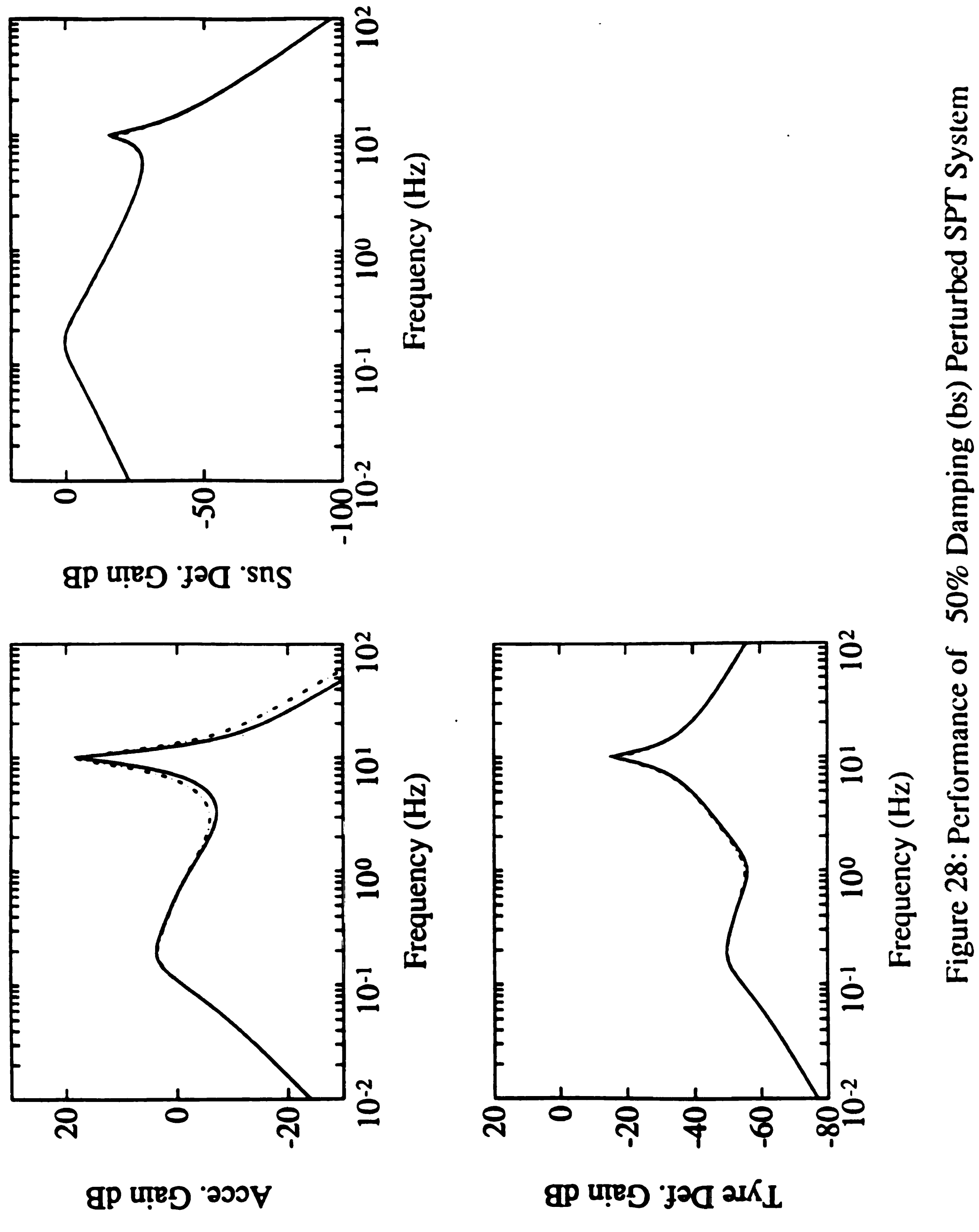

Figure 28: Performance of 50% Damping (b_s) Perturbed SPT System

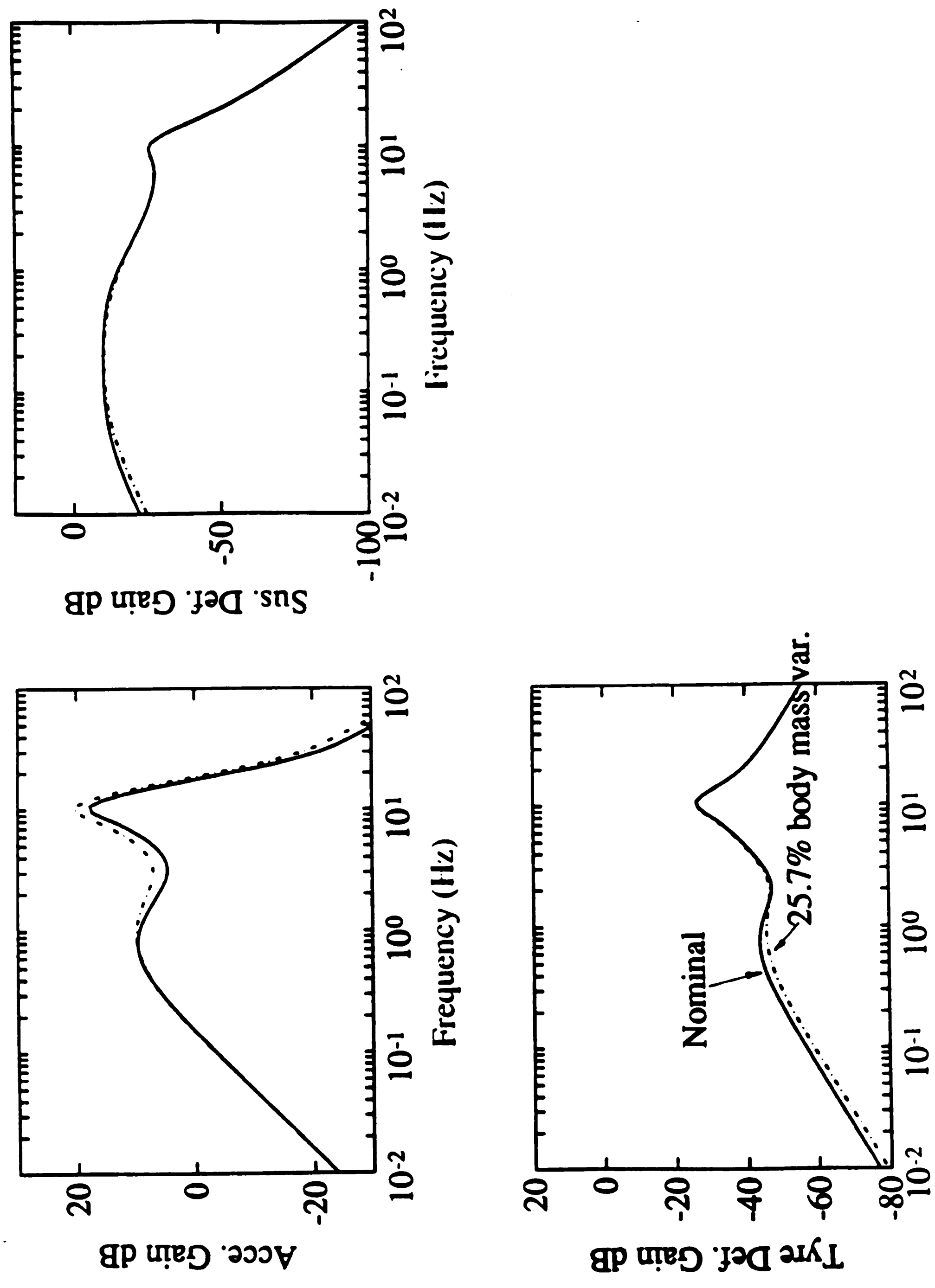

Figure 29: Performance of 25.7% Body Mass (ms) Reduced LQG-P System

Figure 29: Performance of 25.7% Body Mass (m_s) Reduced LQG-P System

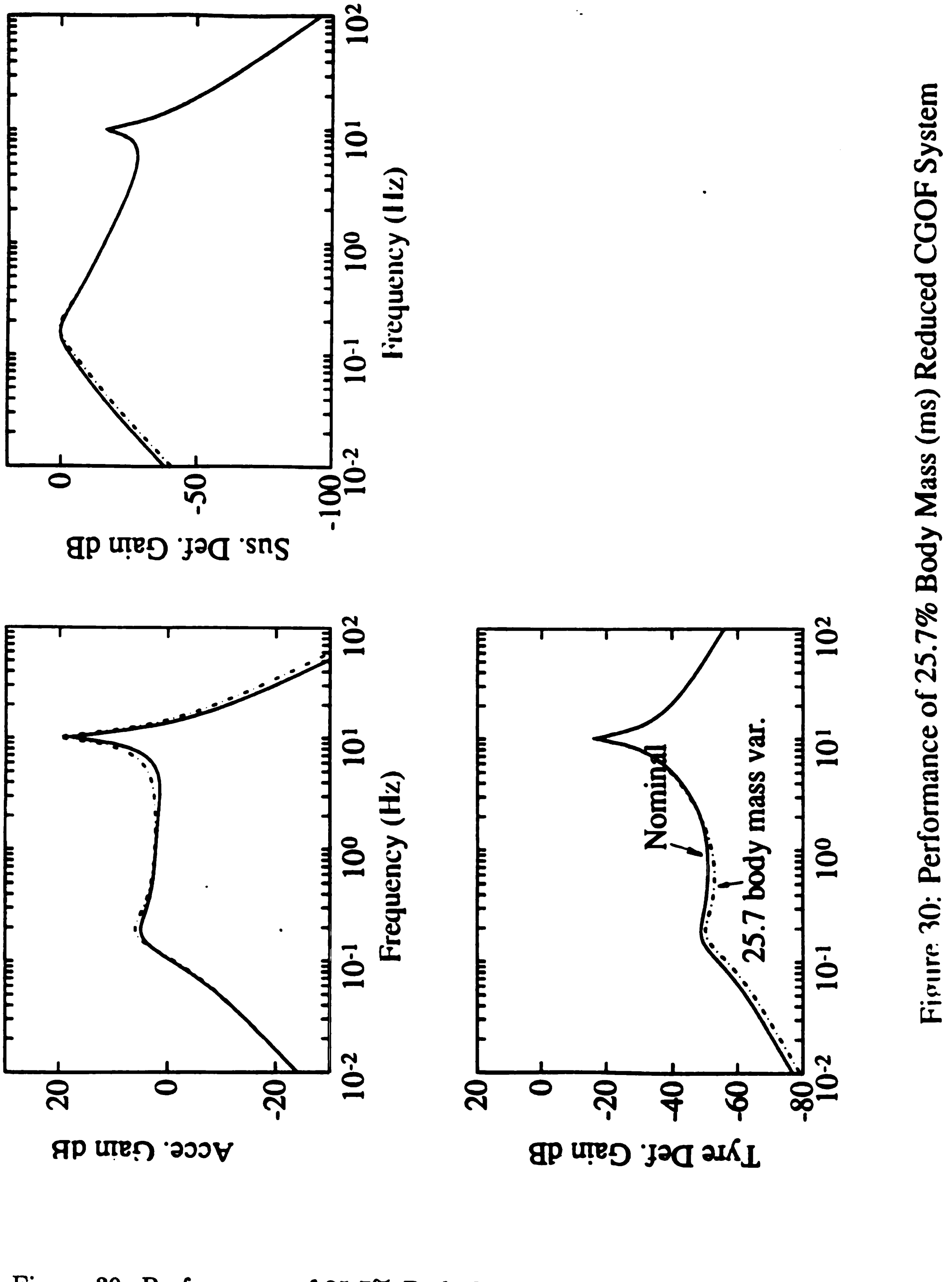

Figure 30: Performance of 25.7% Body Mass (m_s) Reduced CGOF System

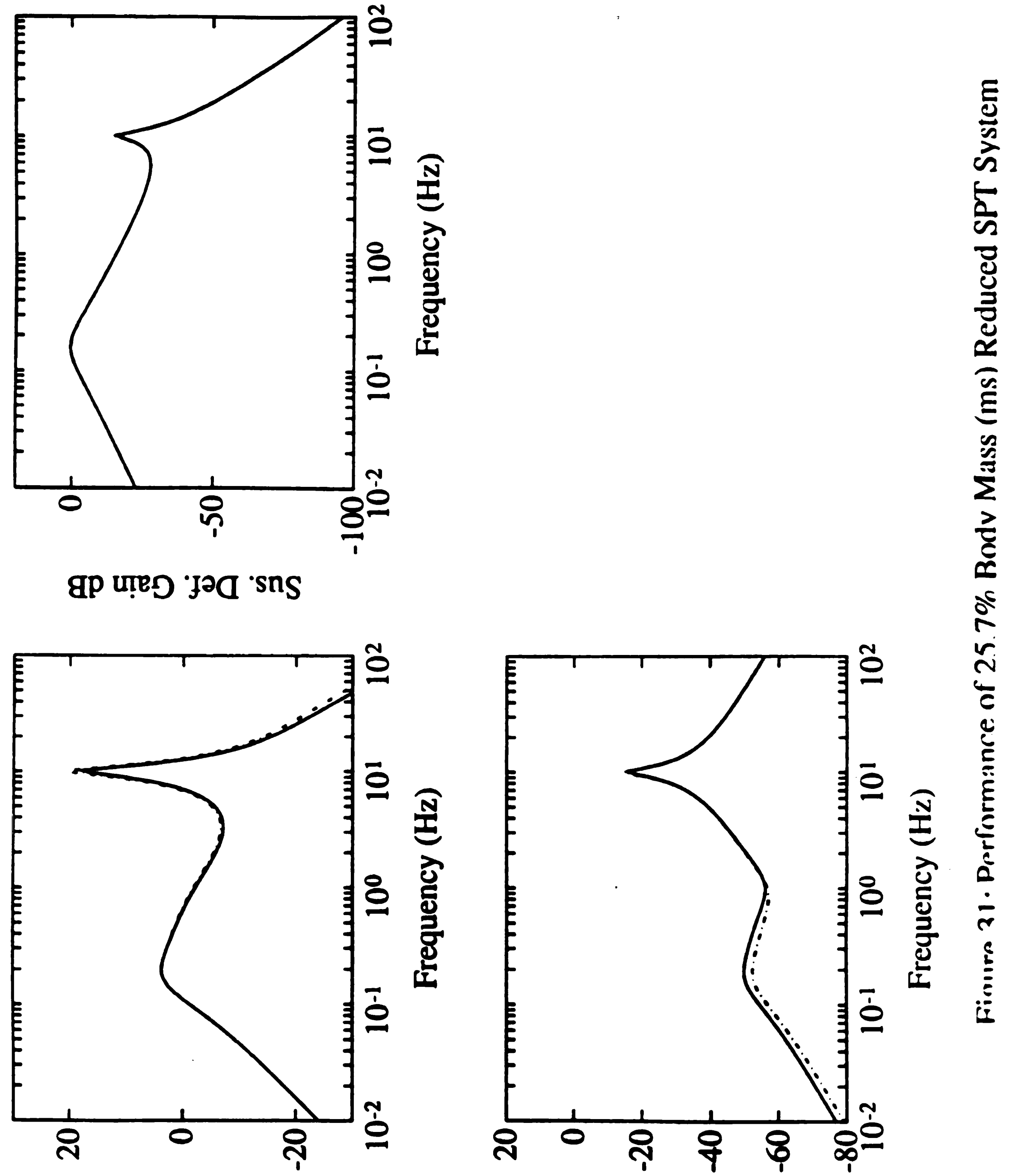

Figure 31: Performance of 25.7% Body Mass (m_s) Reduced SPT System

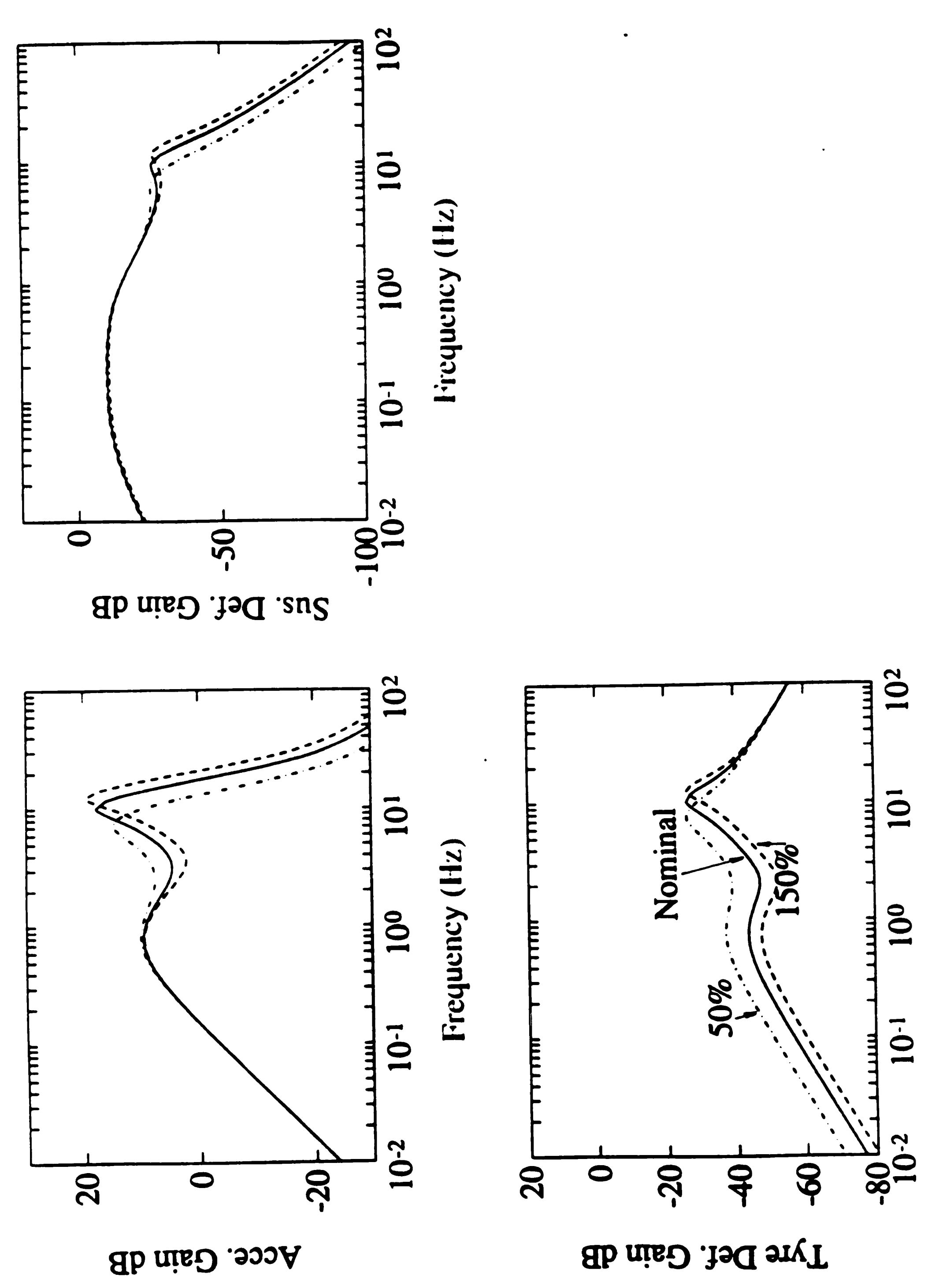

Figure 33: Performance of 50-150% Tire Stiffness (kt) Perturbed LQG-P System

Figure 32: Performance of $50 - 150\%$ Tire Stiffness (k_t) Perturbed LQG-P System

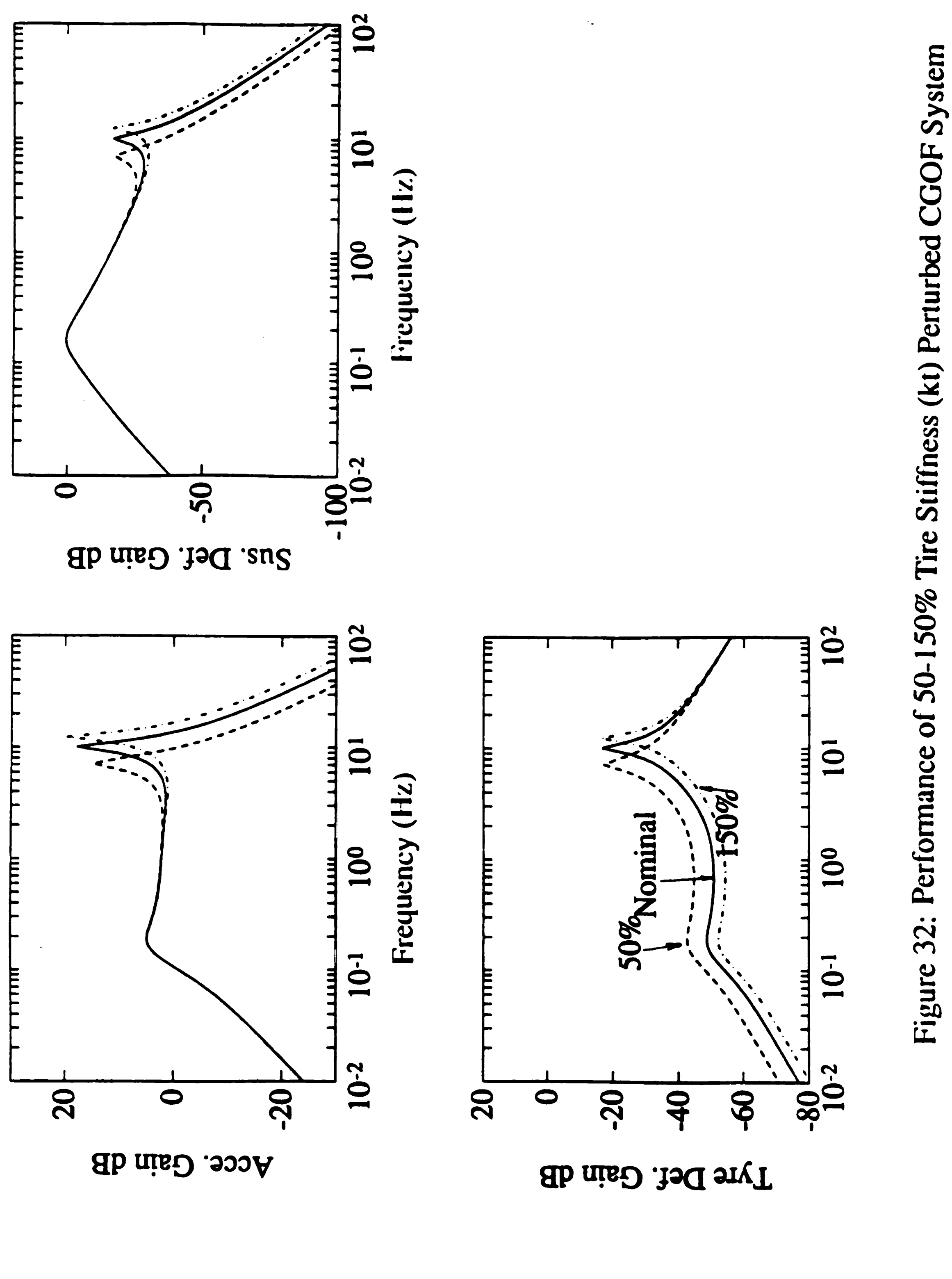

Figure 33: Performance of 50 – 150% Tire Stiffness (k_t) Perturbed CGOF System

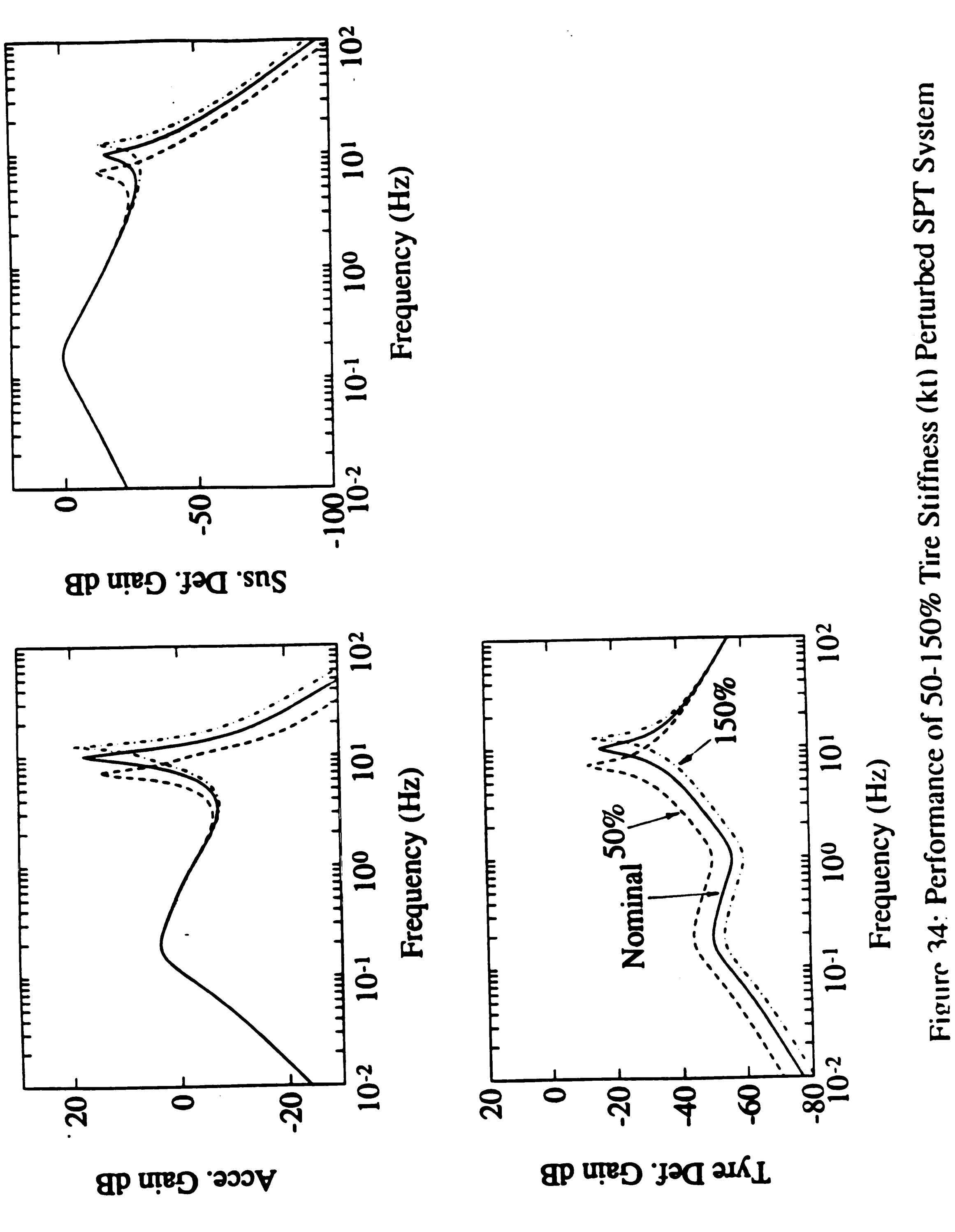

Figure 34: Performance of 50 – 150% Tire Stiffness (k_t) Perturbed SPT System

Appendix A

Through physical understanding of the state variables, it might be easy to conjecture that the state variables related to sprung mass dynamics, i.e., $z_s - z_u$ & $\dot{z}_s$, are slow variables; while the other two state variables related to unsprung mass dynamics, i.e., $z_u - z_r$ & $\dot{z}_r$, are fast variables. This conjecture can be confirmed by modeling the system in the singularly perturbed form. Consider the vehicle state equation as defined before,

$$\dot{x} = Ax + Bu + E\dot{z}_r \tag{A.1}$$

where

$$A = \begin{bmatrix} 0 & 1 & 0 & -1 \\ -k_s/m_s & -b_s/m_s & 0 & b_s/m_s \\ 0 & 0 & 0 & 1 \\ k_s/m_u & b_s/m_u & -k_t/m_u & -b_s/m_u \end{bmatrix}, B = \begin{bmatrix} 0 \\ 1/m_s \\ 0 \\ -1/m_u \end{bmatrix}, E = \begin{bmatrix} 0 \\ 0 \\ -1 \\ 0 \end{bmatrix} \tag{A.2}$$

Let $\epsilon = \frac{\sqrt{k_s/m_s}}{\sqrt{k_t/m_u}}$ and choose a new state vector $\hat{x}$ and a new input $\hat{u}$ as

$$\hat{x} = \begin{bmatrix} \hat{x}_1 \\ \hat{x}_2 \\ \hat{x}_3 \\ \hat{x}_4 \end{bmatrix} = \begin{bmatrix} z_s - z_u \\ \sqrt{m_s/k_s}\dot{z}_s \\ (z_u - z_r)/\epsilon \\ \sqrt{m_s/k_s}\dot{z}_u \end{bmatrix}, \hat{u} = \frac{u}{k_s} \tag{A.3}$$

If we define a new time scale by

$$\hat{t} = t\sqrt{\frac{k_s}{m_s}} \tag{A.4}$$

then, with $(\dot{\ })$ denoting the derivative w.r.t. $\hat{t}$, the state equation is expressed by

$$\begin{bmatrix} \dot{\hat{x}}_1 \\ \dot{\hat{x}}_2 \end{bmatrix} = A_{11}\begin{bmatrix} \hat{x}_1 \\ \hat{x}_2 \end{bmatrix} + A_{12}\begin{bmatrix} \hat{x}_3 \\ \hat{x}_4 \end{bmatrix} + B_1\hat{u} + E_1\dot{z}_r \tag{A.5}$$

$$\begin{bmatrix} \epsilon\dot{\hat{x}}_3 \\ \epsilon\dot{\hat{x}}_4 \end{bmatrix} = A_{21}\begin{bmatrix} \hat{x}_1 \\ \hat{x}_2 \end{bmatrix} + A_{22}\begin{bmatrix} \hat{x}_3 \\ \hat{x}_4 \end{bmatrix} + B_2\hat{u} + E_2\dot{z}_r \tag{A.6}$$

where

$$A_{11} = \begin{bmatrix} 0 & 1 \\ -1 & -b_s/\sqrt{m_s k_s} \end{bmatrix}, A_{12} = \begin{bmatrix} 0 & -1 \\ 0 & b_s/\sqrt{m_s k_s} \end{bmatrix}, B_1 = \begin{bmatrix} 0 \\ 1 \end{bmatrix}, E_1 = \begin{bmatrix} 0 \\ 0 \end{bmatrix},$$

$$A_{21} = \begin{bmatrix} 0 & 0 \\ \epsilon m_s/m_u & \epsilon\frac{b_s}{m_u}\sqrt{\frac{m_s}{k_s}} \end{bmatrix}, A_{22} = \begin{bmatrix} 0 & 1 \\ \epsilon^2\frac{m_s k_t}{m_u k_s} & \epsilon\frac{b_s}{m_u}\sqrt{m_s/k_s} \end{bmatrix},$$

$$B_2 = \begin{bmatrix} 0 \\ -\epsilon\frac{m_s}{m_u} \end{bmatrix}, E_2 = \begin{bmatrix} -1 \\ 0 \end{bmatrix}, \tag{A.7}$$

For the typical numerical parameters given in Table 1.1, ϵ is about 0.1 and all the following quantities are $O(1)$.

$$-b_s/\sqrt{m_s k_s}, b_s/\sqrt{m_s k_s}, \epsilon m_s/m_u, \epsilon\frac{b_s}{m_u}\sqrt{\frac{m_s}{k_s}}, \epsilon^2\frac{m_s k_t}{m_u k_s}, \epsilon\frac{b_s}{m_u}\sqrt{m_s/k_s}, -\epsilon\frac{m_s}{m_u}$$

This shows that the model (A.5)–(A.6) is in the standard singularly perturbed form, and confirms the conjecture that $z_s - z_u$ & $\dot{z}_s$ are the slow variables while $z_u - z_r$ & $\dot{z}_r$, are fast variables. To put the system into the standard singularly perturbed form, we needed to scale some of the state and input variables. Scaling of state variables does not affect the input-output tansfer functions since it is an internal similarity transformation. Scaling of the input only multiplies the transfer function by a constant. Since the sequential design procedure uses transfer function models in designing the controllers, it is not necessary to model the system in the standard singularly perturbed form. It is sufficient to recognize the slow and fast variables and order the components of state vector so that the slow variables come first. Then, the slow and fast models can be defined as in Section 4.1. It can be verified that scaling of state variables does not affect the slow and fast transfer functions.

Bibliography

[1] Hedrick, J.K. and Wormley, D.N.,*ASME AMD*, Vol.15,1975, p.21.

[2] Majeed, K.N., "Centralized/Local Output Feedback Control and Robustness with Application to Vehicle Active Suspension System," *Ph.D. Thesis, U. of Dayton*, 1989.

[3] Alanoly, J., "New Concept in Semi-active Vibration Isolation," *J. Mech. Trans. Auto. Des.*, Vol. 109, June 1987, pp.242–247.

[4] Alanoly, J., "Semi-active Force Generators for Shock Isolation," *J. Sou. Vib*, Vol. 126, Oct. 1988, pp.145–156.

[5] Karnopp, D., "Force Generation in Semi-active Suspensions Using Modulated Dissipative Elements," *Veh. Sys. Dyn.*, Vol. 16, 1987, pp.333–343.

[6] Margolis, D. L., "Chatter of Semi-active On/Off Suspensions and Its Cure,", *Veh. Sys. Dyn.*, Vol. 13, Nov. 1984, pp.129–144.

[7] Hrovat, D., "A Class of Active LQG Optimal Actuators," *Automatica*, Vol. 18, No. 1, 1982, pp.117–119.

[8] Friedland, B., *Control System Design*, McGraw Hill,1986.

[9] Hall, B. B.& Gill, K. F., "Performance Evaluation of Motor Vehicle Active Suspension Systems," *Proc. Instn. Mech. Engrs.*,Vol. 201, No. D2, 1987, pp.135–148.

[10] Karnopp, D., "Two Contrasting Versions of the Optimal Active Vehicle Suspension," *J. Dyn. Sys. Meas. Cont*, Sept. 1986, pp.264–268.

[11] Sharp, R.S., & Crolla, D.A., "Road Vehicle Suspension System Design – a Review," *Veh. Sys. Dyn.*, 16,1987, pp.167–192.

[12] Yue, C., Butsuen, T. & Hedrick, J.K., "Alternative Control Laws for Automotive Active Suspensions," *J. Dyn. Sys. Meas. & Cont.*, Vol. 111, June 2989, pp.286–291.

[13] Miller, L.R., "Tuning Passive, Semi-active and Fully Active Suspension Systems," *Proc. of the* 27^{th} *CDC*, 1988, pp. 2047–2053.

[14] Hrovat, D., "Optimal Active Suspension Structures for Quarter-Car Vehicle Models," *Automatica*, Vol. 26, 1990, pp.845–860.

[15] Elemandy, M.M., "Optimal Linear Active Suspension with Multivariable Integral Control," *Veh. Sys. Dyn.*, 19, 1990, pp.313–329.

[16] Thompson, A.G., "Optimal and Suboptimal Linear Active Suspensions," *Veh. Sys. Dyn.*, 13, 1984, pp.61–72.

[17] Margolis, D.L. "The Response of Active and Semi-active Suspensions to Realistic Feedback Signals," *Veh. Sys. Dyn.*, 11,1982, pp.286–291.

[18] Khalil, H.K., "Output Feedback of Linear Two-Time-Scale Systems," *IEEE Transactions on Automatic Control*, Vol. AC-32, Sept. 1987, pp.784–792.

[19] Luse, D.W. and Khalil, H.K.,"Frequency Domain Results for Systems with Slow and Fast Dynamics," *IEEE Transactions on Automatic Control*, AC-30, Dec. 1985, pp.1171–1179.

[20] Kokotovic, P.V., Khalil, H.K. and O'Reilly, J.,"Singular Perturbation in Control : Analysis and Design,"*Academic*, New York, 1986.

[21] Salman, M.A., Fujimori, K., Uhlik, C., Kawatani, R. and Kimura, H., "Reduced Order Design of Active Suspension Control," *Proceedings of the* 27^{th} *CDC*, Dec. 1988, pp.1038–1043.

[22] Chen, C.T.,*Linear System Theory and Design*, Holt, Reinhart and Winston, 1984

[23] Tahk, M. and Speyer, J.L., "Modelling of Parameter Variations and Asymptotic LQG Synthesis," *IEEE Transactions on Automatic Control*, AC-32, Sept. 1987, pp.793–801.

[24] Yamashita, M., Fujimori, K., Uhlik, C., Kawatani, R. and Kimura, H., "H_∞ Control of an Automotive Active Suspension System," *Proceedings of the* 29^{th} *CDC*, Dec. 1990, pp.2244–2250.

[25] Alexandridis, A.A. and Weber, T.R., "Active Vibration Isolation of Truck Cabs", *Proceedings of ACC*, 1984, pp.1199–1208.

[26] Stein, G. and Athans, M., "The LQG/LTR Procedure for Multivariable Feedback Control Design", *IEEE Transactions on Automatic Control*, AC-32, Feb. 1987, pp.105–114.

[27] Kwakernaak, H., "Robustness Optimization of Linear Feedback System", *Proceedings of CDC*, Dec. 1983.